BRNO UNIVERSITY OF TECHNOLOGY
VYSOKÉ UČENÍ TECHNICKÉ V BRNĚ

FACULTY OF CHEMISTRY
FAKULTA CHEMICKÁ

INSTITUTE OF MATERIALS SCIENCE
ÚSTAV CHEMIE MATERIÁLŮ

EFFECT OF ACTIVATOR NATURE ON RHEOLOGY AND SURFACE CHEMISTRY OF ALKALI-ACTIVATED SLAG

VLIV TYPU AKTIVÁTORU NA REOLOGII A POVRCHOVOU CHEMII ALKALICKY AKTIVOVANÉ STRUSKY

MASTER'S THESIS
DIPLOMOVÁ PRÁCE

AUTHOR
AUTOR PRÁCE

Bc. Kostyantyn Russkykh

SUPERVISOR
VEDOUCÍ PRÁCE

Ing. Vlastimil Bílek, Ph.D.

BRNO 2021

BRNO UNIVERSITY OF TECHNOLOGY
FACULTY OF CHEMISTRY

Specification Master's Thesis

Project no.:	FCH-DIP1604/2020	Academic year:	2020/21
Department:	Institute of Materials Science		
Student:	**Bc. Kostyantyn Russkykh**		
Study programme:	Chemistry, Technology and Properties of Materials		
Study field:	Chemistry, Technology and Properties of Materials		
Head of thesis:	**Ing. Vlastimil Bílek, Ph.D.**		

Title of Master's Thesis:

Effect of activator nature on rheology and surface chemistry of alkali–activated slag

Master's Thesis:

1. State of the art review
2. Optimization of pastes with different activators enabling their mutual comparison
3. Study of rheological properties of the prepared pastes and comparison of results with their surface chemistry (zeta potential)
4. Application of other methods and discussion of obtained results

Deadline for Master's Thesis delivery: 30.7.2021:

Master's Thesis should be submitted to the institute's secretariat in a number of copies as set by the dean This specification is part of Master's Thesis

Bc. Kostyantyn Russkykh Student	Ing. Vlastimil Bílek, Ph.D. Head of thesis	doc. Ing. František Šoukal, Ph.D. Head of department

In Brno dated 1.2.2021

prof. Ing. Martin Weiter, Ph.D.
Dean

ABSTRAKT

V této závěrečné práci bylo popsáno časné reologické chování alkalicky aktivované strusky, anorganického materiálu, který vzniká aktivací mleté granulované vysokopecní strusky alkalickým roztokem. Vliv typu aktivačního roztoku (hydroxidů, křemičitanů a uhličitanů) a jeho koncentrace na časné reologické parametry byl zkoumán pomocí amplitudových oscilačních měření. Bylo pozorováno, že typ aktivátoru je hlavním faktorem ovlivňujícím reologické chování alkalicky aktivované strusky. Dále bylo pozorováno, že aktivátory na bázi draslíku vedou ke slabší struktuře (nižší mez kluzu, mez toku a nižší hodnoty viskoelastických modulů) oproti použití aktivátorů na bázi sodíku. To lze vysvětlit rozdíly ve velikosti alkalických iontů. Na rozdíl od ostatních aktivátorů křemičitany způsobovaly zvýšení ztrátového faktoru, přičemž vykazovaly spíše kapalné chování. Z výsledků vyplynulo, že většina aktivátorů má tzv. kritickou hodnotu koncentrace, po jejímž dosažení mají reologické vlastnosti vzorků tendenci se měnit s rostoucí koncentrací. Získané výsledky korelovaly s výstupy zeta potenciálu.

ABSTRACT

The rheological behavior of alkali-activated slag, inorganic materials synthesized by the activation of ground granulated blast furnace slag (GGBFS) with an alkaline solution, is described. The effect of the activating solution composition (alkali hydroxides, silicates and carbonates) as well as its concentration on the rheological parameters was investigated using amplitude sweep tests. Based on the results of the experiments, it was concluded that the type of activator is the prevailing factor affecting the rheological behavior of the activated slag. It was also confirmed that potassium-based activators lead to weaker structure of the pastes (lower yield point, flow point and values of viscoelastic moduli) than sodium-based activators, which, can be explained by differences in the sizes of alkaline ions. Unlike other activators, silicates dramatically increased loss factor and thus changed the behavior of the pastes from solid-like to liquid-like. It is also clear from the experimental results that most activators have a so-called critical concentration, after which the rheological properties of the samples tend to change. The obtained results were correlated with zeta potential measurements.

KLÍČOVÁ SLOVA

Struska, alkalická aktivace, reologie, povrchová chemie.

KEYWORDS

Slag, alkali activation, rheology, surface chemistry.

RUSSKYKH, Kostyantyn. *Vliv typu aktivátoru na reologii a povrchovou chemii alkalicky aktivované strusky*. Brno, 2021. Dostupné také z: https://www.vutbr.cz/studenti/zav-prace/detail/131486. Diplomová práce. Vysoké učení technické v Brně, Fakulta chemická, Ústav chemie materiálů. Vedoucí práce Vlastimil Bílek.

PROHLÁŠENÍ

Prohlašuji, že jsem diplomovou práci vypracoval samostatně a že všechny použité literární zdroje jsem správně a úplně citoval. Diplomová práce je z hlediska obsahu majetkem Fakulty chemické VUT v Brně a může být využita ke komerčním účelům jen se souhlasem vedoucího diplomové práce a děkana FCH VUT.

---

podpis studenta

PODĚKOVÁNÍ

Rád bych poděkoval vedoucímu práce Ing. Vlastimilu Bílkovi, Ph.D., za cenné rady, vstřícnost, poskytnutí materiálů, odborné konzultace při zpracování diplomové práce, a hlavně za jeho trpělivost. Děkuju též mojí rodině, přátelům a kolegům za podporu během celého mého studia.

OUTLINE

2.1 Alkali-activated materials 8
2.2 Alkaline activation 9
2.3 Alkaline activators 10
2.3.1 Alkaline hydroxides 10
2.3.2 Alkaline silicates 10
2.3.3 Alkaline carbonates 11
2.4 Precursors 11
2.4.1 Blast furnace slag 11
2.4.1.1 Processing 13
2.4.1.2 Granulation 13
2.4.1.3 GGBFS properties 14
2.5 Rotational rheology 15
2.5.1 Viscosity 15
2.5.2 Yield stress 16
2.5.3 Thixotropy 16
2.5.4 Rheological models 17
2.6 Oscillatory rheology 19
2.6.1 Viscoelastic characteristics 19
2.6.2 Amplitude Sweeps 21
2.6.3 Time Sweep 23
2.6.4 Frequency Sweep 23
2.7 General approach 24
2.8 Surface chemistry 25
2.8.1 Surface chemistry of GGBFS in water 26
2.8.2 An analysis of the rheological properties of the paste based on the type and dosage of activator 29
2.8.3 An analysis of zeta potential in relation to activator type and dosage. 29
2.8.4 Analysis of the interrelationship between the zeta potential of the slag suspension and the yield stress. 30
3.1 GGBFS composition 33
3.2 Alkaline activators 33
3.3 Mixture preparation 34
3.4 Mini-slump test 35
3.5 Methods and equipment used 35
3.6 Zeta potential 37
4.1 Mini slump test 38
4.2 Rheological behavior of alkali-activated slag 39
4.2.1 Strain controlled test 39

4.2.2 Stress controlled test 43
4.3 Surface chemistry measurements 46
4.3.1 Zeta potential 46
4.4 Conclusion 48

AIM OF THE STUDY

Yet, little has been said about how different types of activators affect the surface chemistry and rheology of alkali-activated slag. The aim of this thesis was to gain an understanding of impact of different alkaline activators and their concentration on rheological properties of alkali-activated ground granulated blast-furnace slag. For this purpose, the aim was the use of still relatively non-traditional approach of oscillatory rheology (amplitude sweep tests). The objectives can be summarized as follows:

1. Literature research
2. Optimization of pastes with different activators allowing their mutual comparison
3. Study of rheological properties of prepared pastes and comparison of results with their surface chemistry (zeta potential)
4. Application of other methods and discussion of the results obtained.

1 INTRODUCTION

It is assumed that the history of cement began in the 8 century BC, when the ancient Etruscan civilization discovered the main component of cement - lime. But already the ancient Romans were the first to come up with a recipe for an astringent and used it for mass construction. The Romans, mixing slaked lime with volcanic ash, obtained a building material that could remain durable under water. This is how the first hydraulic cement appeared, as can be seen by visiting the Roman Forum or the Colosseum [1]. According to Professor Joseph Davidovits, the Pyramid of Cheops in Egypt was built of concrete [2].

However, the history of modern cement is usually considered based on the date October 21, 1824, when Portland cement appeared thanks to Joseph Aspin. It is named after the city of Portland, where natural stone is mined, which is the same color as Portland cement. Over time, Portland cement has become one of the most popular types of cement.

The production of Portland cement is associated with a high consumption of natural mineral raw materials and energy resources and is accompanied by high volumes of emissions into the environment. One of the main directions of development of the construction industry is the preservation of natural resources by increasing the use of industrial waste. Thus, the question of finding materials alternative to Portland cement is relevant [3].

That is why the development of existing and creation of new binders of alkaline activation based on mineral additives of natural and technogenic origin is of relevance today. At the same time, alkaline activation binders have advantages not only due to the involvement of industrial by-products, but also due to good mechanical characteristics and durability.

However, rheological properties of alkali-activated binders is very complex and often very different to that of Portland cement. One of the most crucial factors affecting rheology and performance of alkali-activated binders is the nature and concentration of alkaline activator. Hence, comparison of various activators at wide range of concentrations is the main motivation for this thesis.

2 THEORETICAL PART

2.1 Alkali-activated materials

Alkali-activated materials are binders that can be produced from a wide range of aluminosilicate precursors. The versatility of AAMs results from the extensive variety of aluminosilicate precursors. Due to the wide variety of aluminosilicate precursors, not only does it differ in availability and price around the world, but also in reactivity. This implies that alkali-activated materials are not universally substituted for building materials, but rather are typically used as a part of a broader set of cements [1].

Alkali activation refers to the reaction of aluminosilicate under alkaline conditions caused by an alkali activator to produce a solid binder based on a mixture of hydrated alkali aluminosilicate [1; 4].

Alkali-activated materials can be produced in two ways: dry powder combined with water, i.e., a one-component mixture, or liquid activator, i.e., a two-component mixture. Today, most products are produced with a two-component mixture, where the handling of chemicals as well as solidifying of materials can be carefully controlled. Although because the one-component mixture can be distributed as a tamped material, it is expected that one-component systems will become a more widely used technology in the future [3].

Common aluminosilicates such as blast furnace slag, coal ash, calcined clays and natural pozzolans are used as precursors for alkali-activated materials. For example, to activate blast furnace slag with alkali, it must be first ground granulated to obtain reactivity. Materials of a hydraulic nature, such as iron-rich clays, cooled and finely ground to reactivity slags from various metallurgical processes, clay-rich wastes from kaolin refining, red mud, ground coal ash, and fly ash are also precursors for alkaline activation.

The most popular alkaline activators are alkali metal hydroxides and silicates. Salts of weak acids can also be effective for activation of precursors with high calcium content, such as blast furnace slag [5].

Alkali-activated materials can be used in:

- reinforced concrete.
- regular concrete
- precast concrete components (including lightweight elements), both reinforced and unreinforced, including pipes
- mortars, grouts and plasters
- foamed and lightweight concretes
- matrices for immobilization of toxic and nuclear waste, both organic and inorganic

In order to produce AAMs, similar production techniques can be used as those involving OPC concrete since precursors and activators are produced using existing processes. Mixtures of AAMs can be manufactured using the same approach used for production of aggregates for OPC concrete. However, the binder must be developed and optimized on a case-by-case basis, since the precursors, depending on their availability in a particular location, will differ in their

chemical and mineralogical composition, which in turn will affect how they are combined with the activators. Therefore, each precursor obtained from different source must be optimized. The characteristics as well as the quality of precursors obtained from industrial by-products must be monitored to produce quality AAMs [1].

The curing of AAMs is similar to the curing of Portland cement-based materials. For example, alkali-activated slag hardens quickly, therefore special hardening retarders are sometimes applied. Depending on the activator dose and the water content of the fly ash-based materials, thermal hardening is used to accelerate the setting process under laboratory conditions. When curing AAMs, a sealed space is also desirable, since curing in water leads to activator washout and curing in a dry space leads to various cracks [3].

The main challenge in the application of AAMs in construction is the development of effective additives to control the rheology in these systems. Some improvement in performance can be achieved by adding some organic compounds, but the rheology of OPC concretes when superplasticizers are added is not up to par [4].

2.2 Alkaline activation

Alkaline activation is a revolutionary discovery in cement science. Victor Glukhovsky suggested that alkali metal compounds of the first group of the periodic chemical table exhibited hydraulic binding properties similar to those exhibited by alkaline-earth metal compounds. His idea of using alkaline compounds as cementitious systems is based on geological data about the presence in the Earth's crust of sodium, potassium and calcium aluminosilicate compounds that have increased resistance to atmospheric reagents. Also, using experimental observations, it was found that hydroxides and salts of alkali metals interact with clay minerals, aluminosilicate glasses and crystalline substances of natural and artificial origin with the formation of water resistant alkaline and alkaline earth aluminosilicate hydration products, which are analogs of natural minerals such as zeolites [1].

According to Krivenko, traditional aluminosilicate cements are capable of hydration due to their ability to convert aluminum-silicon-oxygen tetrahedrons into a discrete state. The resulting hydrates are further capable of polycondensation with the formation of gels - colloidal solutions and, subsequently, crystalline formations [4].

Dissolution consists in the breaking of ionic (Ca-O) and covalent (Si-O-Si, Al-O-Al and Al-O-Si) bonds. For example, in Portland cement, this is due to the blocking of the discrete state of SiO_4 by the Ca ion (e.g., C_3S, C_2S). Because of the protonation of the Ca-O bond, when the mineral is mixed with water, its autocatalytic destruction occurs, with the formation of hydrated $[SiO_4]^{4-}$ and $[AlO_4]^{5-}$ tetrahedrons as well as, $Ca(OH)^+$ or $Ca(H_2O)OH^+$. When the hydration of minerals with low bond ionicity (for example calcium silicate - CS) takes place, where covalent bonds predominate, the ionic strength of water (pH = 7) is insufficient to break the covalent bond. It is possible to alter the ionic strength of the mixing medium by adding alkali metal ions, which have good electron donor properties [4].

2.3 Alkaline activators

An activator plays a crucial role in determining the rheological behavior of the AAS paste. Glukhovsky identified six major categories of compounds in his study, to which activators are classified (M = Na, K):

- alkali metal hydroxides (MOH),
- weak acid salts (M_2CO_3, M_2SO_3, M_3PO_4, MF),
- waterglass (silicates M_2O-nSiO_3),
- aluminates (M_2O-nAl_2O_3),
- aluminosilicates (aluminosilicates mixed with an alkali metal M_2O-Al_2O_3-(2-6) SiO_2),
- strong acid salts (M_2SO_4, MCl) [1].

2.3.1 Alkaline hydroxides

Activators play a very important role in the activation process. Although most studies have focused on the effects of sodium and potassium hydroxides and silicates, it is the potassium hydroxide KOH that usually shows reaction products with better characteristics than NaOH. The larger potassium ion K^+ promotes the formation of large silicate chains with which the aluminum hydroxide ion tends to bind. So, using KOH solutions will cause more activated suspension to form, resulting in faster setting than substances made from NaOH. Depending on the activator, the concentration is optimal. It is known, for instance, that increasing the activator concentration beyond a certain alkali content does not result in further improvement in material performance, but instead causes unfavorable effects. Brittleness and efflorescence, for example, can be observed when a material is exposed to large levels of free alkali [5].

2.3.2 Alkaline silicates

The presence of soluble silicates (or so-called waterglasses) can increase the rate of reaction and as a result improve the characteristics of the final product. The composition of an alkaline silicate solution can be expressed by two parameters: one is the modulus of the solution, which is the SiO_2/Na_2O ratio, and the other is the SiO_2 or M_2O content, or the sum of SiO_2 + M_2O [5]. Silicate modulus is an important characteristic of the chemical composition of both soluble and liquid glass. Commercial liquid sodium silicates have a modulus of 1.6-3.85. Liquid sodium silicates outside this range have limited stability and are impractical. The pH value is the most important characteristic that determines the stability of a high modulus silicate solution [5].

2.3.3 Alkaline carbonates

Yuan et al. states that sodium carbonate Na_2CO_3 is the second activator after liquid sodium silicate that gives the highest mechanical strength [6]. In spite of the many advantages sodium silicate as an activator has in AAS, it has been affiliated with rapid setting in many reports. Jimenez et al. state that rapid slag setting of sodium silicate-activated slag results from the formation of calcium silicate hydrate, while the slow slag setting of Na_2CO_3-activated slag is due to the initial formation of calcium carbonate [7].

Even though alkaline carbonates show promise as activators, the mechanism underlying their action and impact are yet to be fully understood. Additionally, to the previously mentioned publication, the reaction mechanism of potassium/sodium carbonate activation of BFS has been extended, where it is stated that M_2CO_3 (M = Na, K) maintains a buffer alkaline environment during the activation reaction [8].

2.4 Precursors

The alkali-activated materials are usually prepared from common aluminosilicates such as blast furnace slag, coal ash, calcined clays, or natural pozzolans. Using blast furnace slag as an example, it must be granulated to obtain reactivity by activating with alkali. As well as clays of a hydraulic nature, cooled and finely ground slags from various metallurgical processes, wastes from kaolin refining, red mud, ground coal ash, and fly ash are precursors to alkaline activation.

2.4.1 Blast furnace slag

Blast furnace slag is a secondary product which is produced in the blast furnace concurrently with pig iron shown in fig.1. Its compound mainly consists of calcium silicates, aluminosilicates, and other bases which are developed sequentially with iron in a blast furnace in an igneous condition.

The blast furnace receives a charge in certain proportions, where iron ore is used as starting material and coke as fuel and reducing agent. Furthermore slag-forming materials, mainly limestone and dolomite, are added there, to improve the iron, and to get rid of certain substances, such as sulfur and phosphorus. As a result, because of the different densities, a film of molten slag forms on the molten iron, which in turn interferes with the oxidation of the iron. During the release of smelting products, liquid iron and slag come out of the blast furnace. The liquid slag rushes down the slag chute to the slag train and further to the slag granulation unit [9]. A granulation process can be used to cool and fragment molten slag, in which jet streams of water and air or pressure are applied to the slag. As an alternative, the liquid slag is partly cooled by water and released into the air with rotating drums. To obtain the required reactivity, it is necessary to ground the obtained slag fragments to perfection almost the same as ordinary Portland cement. Typically, the glass content of slags ranges from 70-99% and depends on how the cooling is initiated and at what temperature it is operated. Glass is a guarantee of latent hydraulic slag because crystallization produces crystals that do not react with water [10].

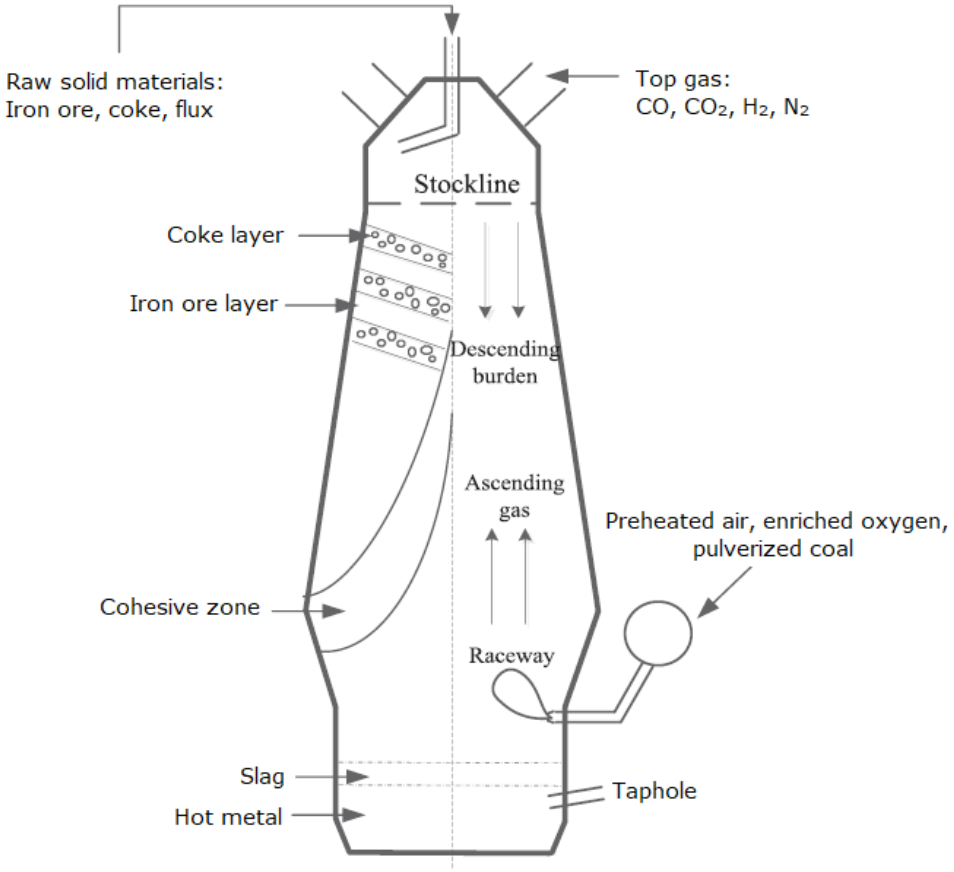

Figure 1: A brief diagram of the blast furnace.

The chemical composition of slag is very important to improve the hydraulic activity of slag. The composition of blast furnace slag varies depending on the flux stone, ores, and various impurities in the coke supply to the blast furnace. Typically, the composition of blast furnace slag is over 95% silica, calcium, aluminum, magnesium, and oxygen [11].

Iron or iron oxides are not the main components of blast furnace slag. It is important that the iron in the slag is not in the form of oxide but instead in the form of highly reduced metallic iron (pig iron). Therefore, slags can be classified into their basicity index.

$$M_z = \frac{CaO + MgO}{SiO_2 + Al_2O_3} \qquad \text{Eq. (1)}$$

CaO/SiO_2 ratio is the simplest basicity indices. Basicity index is the ratio of basic oxides to acidic oxides. If the Basicity index is greater than 1 the slag is alkaline, if the modulus is less than 1 the slag is acidic. It is necessary that calcium over siliceous oxide ratio must be greater than 1. Hydraulic activity depends on the basicity of the slag, the more basic the slag, the greater its hydraulic activity in the presence of alkaline activators.

2.4.1.1 Processing

Unlike conventional primary products, such as conventional building materials, or ordinary Portland cement, which are produced under carefully controlled conditions, blast furnace slag is a byproduct with lower costs for its further use in construction. As blast furnace slag cannot be produced in a way that strictly complies with technical specifications, it will have varying physical and chemical properties. Therefore, slag processing that meets quality control requirements is an important component in obtaining quality slag [10].

The characteristic differences in the composition and chemical properties of blast furnace slag are highly dependent on the production process. Depending on the different deposits of iron ores or the composition of recycled steel scrap, the composition of the main raw material - iron - also changes. Chemical and physical properties of flux materials can also significantly affect the refining process and subsequently the properties of blast furnace slag.

Accordingly, to convert slag from a by-product into a quality product for further use in various applications, slag processing with strict quality control is necessary. Processing techniques include cooling, mechanical crushing and screening [10]. The method of cooling and processing can physically affect the final product. For example, blast furnace iron slag can be processed into air-cooled slag, pelletized slag, expanded, and pelletized slag. However, this work focuses on granulated blast furnace slag, so it is the granulation process that will be discussed in detail further.

2.4.1.2 Granulation

It is known that historically blast furnaces produced about one ton of slag per one ton of pig iron. The large quantity of slag made it difficult to dispose of, so it was taken to special dumps where it was accumulated. However, due to the fact that at the end of the nineteenth century the binding properties of slag were discovered, in the middle of the twentieth century granulated slag was produced from blast furnace slag.

The granulation process is used to turn liquid blast furnace slag into raw materials for cement and concrete by combining blast furnace slag with water. There are two types of slag granulation: wet granulation and air granulation. The whole process takes place in a slag granulation plant. The granulation plant consists of a granulation section, a dewatering and a storage section, but it is in the granulation section that various granulation processes take place [12].

In the wet process, liquid slag is fed through a runner to the granulation plant to produce traditional water granulated blast furnace slag. Then, the liquid slag stream at around 1500 ºC is discharged into a high-speed water stream and then enters the granulation basin at around 50 ºC. Thus, the traditional wet granulation process produces a mixture of water and granulated slag of approximately 5 mm in size [12]. In air granulation, a pelletizer is used. The molten slag is fed to a vibrating feed plate, where water is sprayed due to rapid heat exchange between molten slag and water, and the slag cools down and expands. The slag then enters the rotating drum, which by rotation sends the slag into the air, where the slag solidifies and turns into round granules [12].

Then the granulated blast furnace slag is milled to produce ground slag. Ground slag is a product obtained by fine grinding of granulated blast furnace slag together with hydrophobic

additive (or without it) intensifying grinding and providing its safety during storage and fluidity during transportation. Fine grinding of ground slag is carried out with any grinding unit, providing the required parameters of the final product. Ground slag is used as a hydraulic binder for alkali activation [11].

2.4.1.3 GGBFS properties

GBFS is a granular, amorphous material of an almost white color, which in finely ground form has hydraulic cementitious properties. The average particle size depends on many factors and varies in the range of 2 mm. For example, the average particle size is determined by the rotational speed of the drum [12]. In the air method of granulation, more particles with smaller size appear at high rotational speed, resulting in a low average diameter. However, high rotational speeds require a large diameter dry granulation device, which can result in high slag processing costs. The shape of the particles can also vary from sharp-angle-free, though not smoothly rounded, to somewhat rounded. The reactivity of GBFS depends on the fineness of its particles and is measured by the specific surface area. Increasing fineness contributes to increased strength, but at the same time fineness depends on a variety of operational factors. The average value of the specific surface area differs from country to country, but is in the range of 0.4 - 0.5 m^2/g. The glass content of the slag is also an important variable. The range of glass content also varies from country to country and can range 70-99%. It should be noted that the glass content of the BFS is inversely proportional to the particle diameter value - as the glass content of the BFS decreases, an increase in the particle diameter of the slag can be observed [12].

The chemical properties of BFS depend on the composition of raw materials.

Table 1: typical chemical analysis results of GBFS obtained from national slag association (NSA, 2016)

SiO_2	Al_2O_3	Fe_2O_3	MnO	CaO	SO_3	K_2O	Na_2O
27 – 38	7 - 15	0.2 - 1.6	0.15 - 0.76	34 - 43	> 0.07	0.08 – 1.83	0.2 – 0.48

Although blast furnace slag has both crystalline and glass phases, the cementing nature of granulated blast furnace slag directly depends on the glass content. Only when GBFS is rapidly cooled, it becomes glassy material. Only when the material is finely ground into a fine powder then the strong adherence of the binders is achieved. Because of its properties, GBFS has been used as a component of cement mixtures, a mineral additive, or as an additional cementitious material in OPC concretes. Suspension of granulated blast furnace slag in water has a pH from 8 to 10, which reflects its slightly alkaline nature [9].

2.5 Rotational rheology

Rheology is a branch of physics which is used to describe and assess the deformation and flow behavior of materials. In rheology, the properties of substance refer to the relationship between shear stress and shear rate, and these are the key concepts in rheology. Rheology deals with both the flow characteristics of liquids and the deformation of solids and in particular the behavior of complex viscoelastic materials that have both solid and liquid properties in response to force, deformation, and time.

2.5.1 Viscosity

Viscosity is the physical characteristics that represents the flow resistance of simple fluids. Newton's law of viscosity describes the relationship between the shear stress and shear rate of a fluid under mechanical stress. The ratio of shear stress to shear rate is a constant, for a given temperature and pressure, and is defined as the viscosity or coefficient of viscosity [13]. The fluid that follows this Newton's law of viscosity called Newtonian fluid. Non-Newtonian fluids do not follow Newton's law and, thus, their viscosity (ratio of shear stress to shear rate) is not constant and is dependent on the shear rate. Dynamic viscosity is the coefficient of viscosity as defined in Newton's law of viscosity. Kinematic viscosity is the dynamic viscosity divided by the density [14].

Flows can be categorized into two basic types: shear flow and extensional flow. While shear flow occurs when fluid components shear past one another, extensional flow occurs when fluid components flow away from one another. One of the easiest flow behaviors to measure on a rotational rheometer is shear flow [15].

The model of two plates is usually used to describe the shear flow behavior, where the fluid sample is placed between two plates and the sample itself can be depicted as layers of fluid and each layer is moving faster than the one beneath it. The upper plate is moving at certain velocity, while the bottom plate remains stationary. A shear force must act on the fluid for shear flow to occur. In this case, the role of external force takes the form of a shear stress (σ) which is defined as the force (F) acting over a unit area (A). And while the bottom plate remains stationary, the upper plate will dislocate given the certain distance. This gradient of displacement across the sample is called the shear strain (γ). Flow becomes impossible for solids which behave like a single block of material. However, for a fluid in which the constituent components can be moved relative to one another, shear strain will increase during the applied stress period. At this case, it creates a velocity gradient, referred to as the shear rate or strain rate $\dot{\gamma}$, the rate at which strain changes over time [15; 16].

Shear stress and shear rate are independent quantities of the measuring system. Shear stress τ and shear rate γ are calculated by $\tau = \frac{F}{A}$ and $\dot{\gamma} = \frac{v}{h}$, where shear force F (in N, newton), shear area A (in m^2), velocity v (in m/s) and shear gap h (in m) [15].

2.5.2 Yield stress

Many materials, depending on the applied stress, exhibit properties characteristic of either solids or liquids. When a small stress is applied to a material, the material deforms in an elastic manner, but when a critical value of the applied stress is reached, the material begins to flow. This critical value of applied stress at which the material begins to flow is called yield stress (σ_y) [17].

Determining the yield stress in many industrial processes is of key importance. In concrete, for example, the yield stress determines whether air bubbles will remain within the suspension or "bleeding", which is basically unwanted sedimentation where there is only water on the surface of the sample [18].

Today, a distinction is made between two yield stresses, dynamic and static; the first is determined by the minimum stress required to start flowing, and the second by the lowest stress applied before the specimen stops flowing [17]. For the purposes of this paper, the dynamic yield stress will be considered in theoretical part, however in experimental part the static yield stress will be examined.

2.5.3 Thixotropy

The occurrence of thixotropy is usually related with a physico-chemical occurrence that causes changes in shear stress at constant shear rate, or with the reversed order. It is not straightforward, however, to assign build-up and breakdown entirely to chemical reactions, which occur at the same time. For example, Thixotropic behavior takes place in cases of reversible build-up. The hysteresis loops and static yield stress measurements are deemed as the most common techniques and strategies for measuring the thixotropy and structural build-up (combining thixotropy and workability loss) [15].

It is very important not to confuse thixotropy and pseudoplasticity. For pseudoplastic fluids, viscosity decreases as shear stress increases, whereas for thixotropic fluids, viscosity decreases over time at a constant shear stress until reaches plateau. According to Russel et al. a thixotropic body is one in which [19]:

- When a shear stress or strain rate is suddenly applied and then held constant, the apparent viscosity decreases with time.
- The body returns to its initial state after a sufficient amount of time has passed.

This time-dependent decrease in viscosity can be explained by a reversible change in the microstructure of the suspension during shear. In the absence of shear, the damaged structure is restored. Thus, the yield strength or shear thinning can be considered as a special case of thixotropy when shear damage and structure recovery occur simultaneously.

2.5.4 Rheological models

The flow behavior of different materials can vary. For this purpose, several rheological models such as Bingham, Hershel-Bulkley, Ellis or Casson models have been developed to describe the flow behavior of these materials [19]. This thesis is related to mineral suspensions based on cementitious materials. This type of paste exhibits rheological properties due to the colloidal suspension of fine particles with water between the coarse grains. One of the most critical properties related to the flow behavior of cementitious suspensions is the yield stress. The yield stress is the minimum stress applied to make a material flow. The presence of this kind of stress can significantly affect the flow rate of the non-Newtonian mineral mixture.

As it was mentioned before, there are two main types of fluids: Newtonian fluids and non-Newtonian fluids. Newtonian fluids obey Newton's law of viscosity, which states, that viscosity of Newtonian fluid remains constant regardless of the amount of shear applied. This type of fluids has a linear relationship between viscosity and shear stress. In contrast to Newtonian fluids, non-Newtonian fluids have different properties [19; 20].

Since non-Newtonian fluids do not follow Newton's law, their viscosity (ratio of shear stress to shear rate) is not constant and is dependent on the shear rate. There are a variety of ways in which non-Newtonian fluids respond when stressed - some become more solid while others become more fluid. While some non-Newtonian fluids react in accordance with the amount of stress applied, others react in accordance with the length of time that the stress is applied. These fluids have a non-linear relationship between shear stress and shear rate (shear thinning or shear thickening), a yield stress, or viscosity that depends on time or deformation history (thixotropic fluids), or a combination of all the above [14].

According to the Yahia and Khayat, the yield stress can be used as a quality control index of self-consolidating and self-leveling systems [21]. Yield stress can be determined by calculating the data from shear stress-shear rate with zero shear by using the appropriate analytical rheological model. Besides the fact that there are several rheological models are relatively suitable to describe the behavior of cementitious materials, only the Bingham alongside with Hershel-Bulkley models are the most widely accepted for this purpose [20]. Overall, the Bingham model is generally used to determine the yield stress. However, compared to the other rheological models, Yahia and Khayat state, that for suspensions incorporated with rheology-modifying admixtures and highly pseudoplastic suspensions the Bingham model tends to provide the least appropriate results in terms of fitting experimental shear stress data [21]. On the assumption that yield stress values strongly depend on effectiveness of the rheological model, the Bingham model can produce results which may considerably differ from results obtained by Hershel-Bulkley model [20].

The Bingham model has a linear relationship between shear stress and shear rate and is characterized by an equation (2):

$$\tau = \tau_B + \eta_B \dot{\gamma} \qquad \text{Eq. (2)}$$

Where τ_B is the Bingham yield point and η_B is the Bingham viscosity. According to Mezger, this model is mostly used when the material represents a constant slope above the yield stress [15].

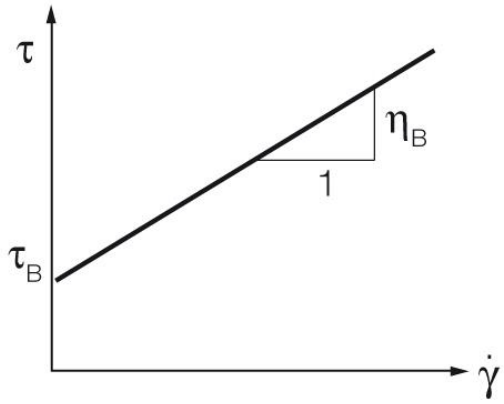

Figure 2: Graphical representation of the Bingham model [15].

According to the physical interpretation of this model, in order to cause a Bingham fluid to flow, some initial effort should be made to initiate the motion to overcome the yield value. With motion or flow initiated, the required force to deform concrete increases with the shear rate increment, which is attributed to plastic viscosity [22].

After all, adding various additives in cementitious suspensions may affect the linear relationships between shear rate and shear stress. Therefore, the modified Bingham rheological model was proposed. As Alonso et al states, by introducing a dimensionless stress correction factor *k*, it is possible to help combat the effect of the Bingham plastic model underestimating stresses at high shear rates and overestimating stresses at lower shear rates [23].

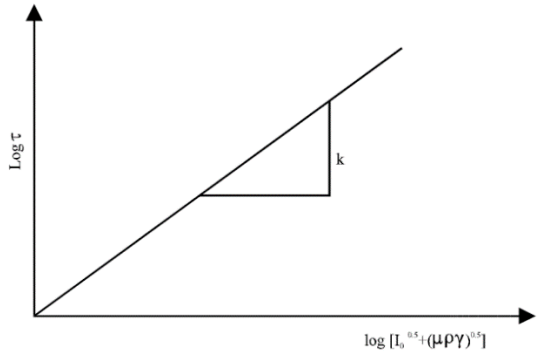

Figure 3: Modified Bingham plastic model rheogram [15].

The Hershel-Bulkley model is an extension of Bingham model, the difference is that it includes shear rate dependence. As stresses are applied above the yield stress, the Hershel-Bulkley equation (see Eq. 3) describes the flow curve of a material with a yield stress and shear-thinning or shear-thickening behavior [15]:

$$\tau = \tau_{HB} + c \cdot \dot{\gamma}^{p} \qquad \text{Eq. (3)}$$

Where τ_{HB} is Hershel-Bulkley yield point, which describes the suspension's yield point, c is Hershel-Bulkley viscosity (consistency index) that describes viscosity at certain shear rate and p is Hershel-Bulkley index which describes the suspension's flow behavior.

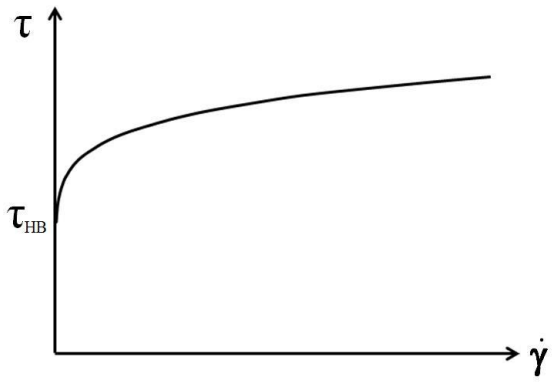

Figure 4: Herschel-Bulkley model for the yield point [15].

Considering the fact, that alkali-activated materials can be prepared using many different precursors such as blast furnace slag, fly ash, metakaolin and chemical wastes and alkaline activators such as alkaline hydroxides, carbonates and waterglasses it is seemed to be a very versatile product. Every compound can affect the rheology of any alkali-activated system. As Alonso et al. state, Hershel-Bulkley rheological model is usually recommended for silicate-activated pastes, when alkali hydroxide-activated paste is more suitable for Bingham model [23].

2.6 Oscillatory rheology

The unique mechanical behavior of material's pastes is a key factor determining their application. The study of the mechanical behavior of such materials is complicated by their viscoelastic response, intermediate between that of solids and liquids. Oscillatory rheology is a suitable experimental tool for studying such behavior; it provides insight into the physical mechanisms that govern the unique mechanical properties of such materials.

2.6.1 Viscoelastic characteristics

To understand the linear (LVE) and nonlinear (NVE) behavior of a material, oscillatory measurements by monitoring the evolution of the complex modulus can be extremely effective. The sample is deformed sinusoidally in shear during this measurement, and its response is measured in terms of shear stress using torque. With the procedure, the signal is converted into shear stress, resulting in a sinusoidal relationship with a phase shift [19].

The phase shift is a certain delay between the response of the sample and the applied shear strain (shown in Figure 5). The phase shift δ can take values from 0 to 90º, where 0º is ideally elastic materials and 90º is ideally viscous materials. Viscoelastic materials take place somewhere in the middle [20].

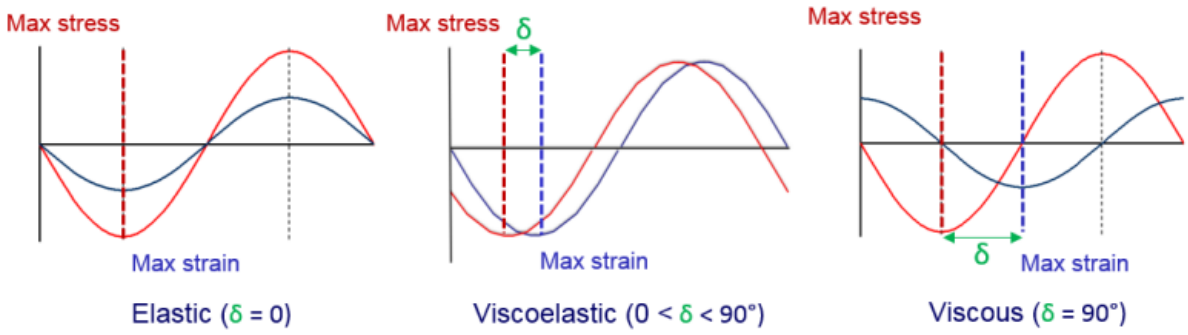

Figure 5: *Stress and strain wave relationships for a purely elastic (ideal solid), purely viscous (ideal liquid) and a viscoelastic material* [24].

The definition of the law of elasticity for oscillatory shear tests is given by an equation 4.

$$G^* = \frac{\tau_A}{\gamma_A} \qquad \text{Eq (4).}$$

Where G* is the complex shear modulus which describes the entire viscoelastic behavior of a sample. Eventually, it is necessary to divide this value into purely viscous and purely elastic components. Figure 6 shows that the elastic response of the sample can be deduced as the storage modulus G′ and viscous response as loss modulus G″. Already mentioned phase shift can be expressed as a ratio between G′ and G″. Storage modulus is the capacity of a material to store strain energy (to return to its original state). The loss modulus is the viscous component, which is a measure of the dissipation of energy through heat due to internal friction during flow. If G′ > G″, the material behaves as a viscoelastic solid. Similarly, if G′ < G″, the material has the character of a visco-elastic fluid [16].

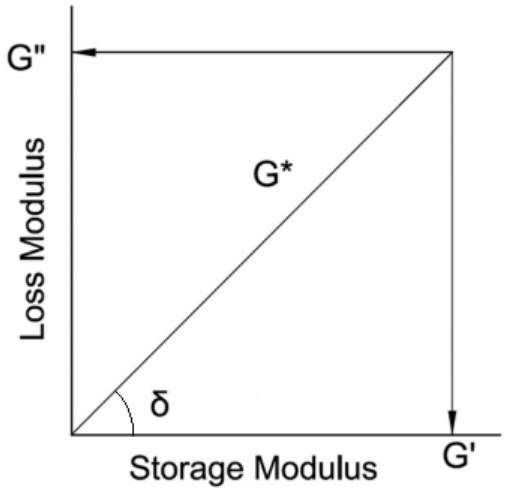

Figure 6: Complex shear modulus (G), storage (G′), and loss (G″) moduli and phase difference (δ)* [25].

The Linear viscoelastic region (shown in Figure 7) (LVE) is the range of shear strain that is applied to a sample without risk of structural damage. Outside this region, irreversible changes

occur. LVE is determined by amplitude-sweep oscillatory measurements at constant frequency and temperature, in which the sample is gradually deformed at certain intervals of increasing strain. The result is a storage and loss moduli on a logarithmic scale as a function of strain

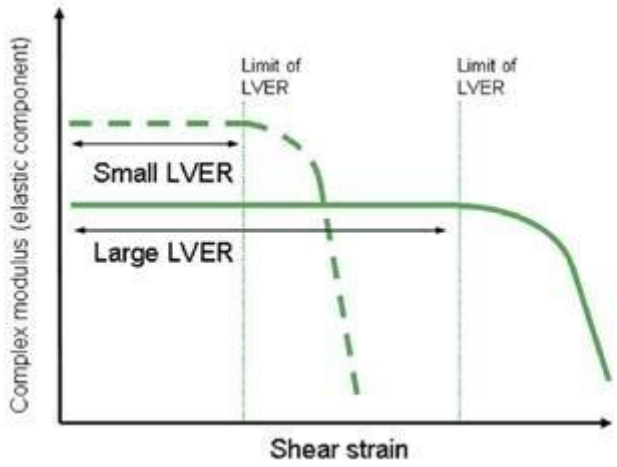

Figure 7: A schematic representation showing how the LVE region is located in the amplitude sweep experiment. (Obtained from: https://www.netzsch-thermal-analysis.com)

2.6.2 Amplitude Sweeps

Amplitude sweeps generally aim at describing the deformation behavior of samples in the non-destructive deformation range and at determining the upper limit of this range. For amplitude sweeps, the deflection of the measuring system is increased stepwise from one measuring point to the next while keeping the frequency at a constant value.

There are two modes of operation for presetting the deflection: a strain sweeps also referred as shear-strain-amplitude sweep, with controlled-shear deformation (CSD) and a stress sweep likewise mentioned as shear-stress-amplitude sweep with controlled shear stress (CSS).

Both stress and strain amplitude sweeps are in most cases carried out to establish the critical strain or stress of cementitious suspension, which mostly correlates to either the end of the LVE or the onset of the flow phase of the cement paste.

In order to understand the measurement results of the amplitude sweep, a diagram is generally used with strain or shear stress plotted on the x-axis and storage modulus and loss modulus plotted on the y-axis on a logarithmic scale.

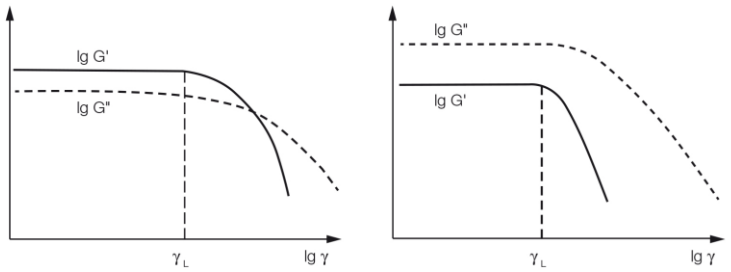

Figure 8: Results of two amplitude sweeps, the functions of G′ and G″ show constant plateau values within the LVE region. Left: G′ > G″ in the LVE region, thus the sample has a gel-like or solid structure. Right: G″ > G′ in the LVE region, thus the sample is fluid [15].

With the aid of a ruler, analysis software, or the data table, it is possible to establish the limiting value, also known as linearity limit, of the viscoelastic region. In order to define the linearity limit (as shown in figure 8), strain is calculated as a percentage with a deviation of 5 to 10 percent accuracy for G′. Aside from these, both storage and loss moduli are also determined. As long as the storage modulus value is higher than the loss modulus value, the sample tends to show a gel-like or solid structure and can therefore be called a viscoelastic solid material. A sample that behaves in the opposite way is said to be viscoelastic liquid and has a fluid structure. One very suitable parameter, related directly to the internal structure of the material, is the flow point. It describes the required force that must be dissipated to make a substance flow [15].

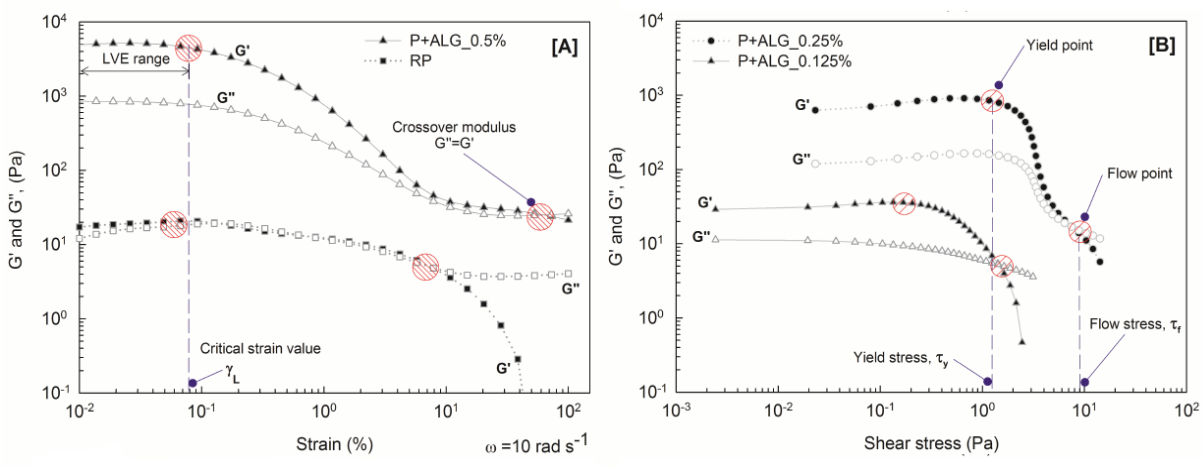

Figure 9: Typical plots of amplitude sweep test results. (A) Storage modulus G' and loss modulus G" against strain amplitude. (B) G′ and G″ against shear stress [27].

An amplitude sweep is usually presented as a graph with strain (or shear stress) plotted on the x-axis and the storage modulus G′ and loss modulus G″ plotted on the y-axis where both axes on a logarithmic scale.

2.6.3 Time Sweep

Time sweep is used to analyze materials such as suspensions and emulsions containing various discrete substances that are randomly distributed in a fluid medium and can undergo macro- or microstructural rearrangement over time. These rearrangements can in turn directly influence the rheological behavior of the sample under study. A time sweep can provide valuable information about how the material changes over time. Also, different information about changes in structure, settling dispersion and time-dependent thixotropy can be obtained depending on the sample to be tested. For a successful experiment, however, the material must be in a stable state [28].

A simple test to determine whether a system has time-dependent rheological properties is the oscillatory time sweep. This test monitors the development of viscoelastic properties after loading over time. During the test, the shear strain amplitude and frequency must be constant. According to Shultz et al., it is preferable to measure controlled shear strain rather than controlled shear stress [29]. The reason for this is that when shear strain occurs, the rheometer applies a specified force in the form of a torque and measures how much the sample is deformed [15].

2.6.4 Frequency Sweep

Frequency sweeps are used to study the time-dependent behavior of samples in a non-destructive range of strains. In this test, high-frequency signals simulate rapid movements in short periods of time, and low-frequency signals simulate slower movements at rest or over prolonged periods [15].

When the deflection is pre-set, there are two ways to operate it:

- Controlled shear deformation,
- Controlled shear stress.

According to the literature [15; 16; 19] it is necessary that the selected shear strain or shear stress amplitude lies within the LVE region. By doing so, an amplitude sweep must first be used to define the LVE region.

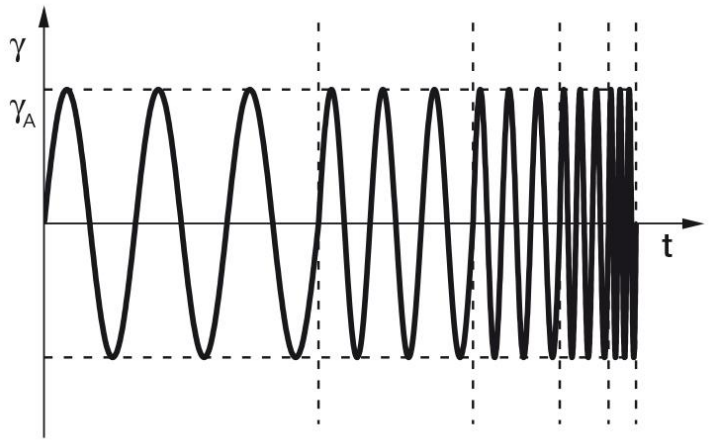

Figure 10: Frequency sweep preset, where a controlled shear deformation is demonstrated by increasing or decreasing the frequency in several steps [15].

The results of frequency sweeps are plotted as a diagram with the frequency on the x-axis and loss and storage moduli on the y-axis, both on a logarithmic scale.

2.7 General approach

Currently, rotational and oscillatory tests are used as the most commonly used techniques to evaluate the rheological characteristics of cement paste.

Since cement pastes are fluids with a yield stress, it should be assumed that material flow begins as soon as the applied stress exceeds the yield stress. Shear thickening or shear thinning paste behavior heavily depends on the suspension consistency and applied shear rate (or shear stress). An appropriate testing procedure is usually chosen based on the investigated material properties, such as steady flow, thixotropic or viscoelastic behavior during rotational or oscillating experiments. A few preliminary tests are used to analyze the response of the suspension to deformation and only then a specific testing approach is determined.

Rotational tests usually involve viscosity functions based on shear rate, shear stress and time. Testing is done either step-by-step, with a couple seconds between every increment of shear rate or stress, or linearly. Most often, either the up and down parts of the loop curve are completed, or only the decreasing portion. Depending on the applied rheological model, the downward branch calculates rheological properties. The result of a rheological tests can be presented as a curve flow diagram displaying the resulting shear stress values, and as a viscosity function. In terms of flow properties, a material can distinguish between ideal viscous behavior, shear-thinning, and shear-thickening [16].

2.8 Surface chemistry

By varying rheological properties such as yield stress and apparent viscosity, the flow behavior of the AAS paste can be controlled. Generally, a paste with a low yield stress is a more desirable result because it improves the ability to fill voids when the concrete is placed. Also, according to Kashani et al., it is important to avoid increasing the yield stress during early age reaction, which in turn leads to thickening and curing of the paste [30]. In the case of Portland cements, this is controlled by various organic additives or plasticizers [31]. However, this is not an effective solution because a specific chemical additive must be developed for each specific cement material. Nevertheless, high yield stress is desirable in some specific publications such as 3D printing.

The addition of an alkaline activator increases the pH and also provides a different electrolyte environment in the fresh binder. A consequence of this is differences in the surface charges of the particles. Zeta potential measurements are used to monitor such changes. It is the measurement of the electrical forces of the double layer using the zeta potential that informs about the most key parameters determining the yield strength [29].

Thus, referring to the study conducted by Hamada et al., we can learn that the use of alkali hydroxide activators in AAS pastes contributes to an increased yield stress [31]. Also, compared to alkali silicate activators, alkali hydroxide promotes a rapid increase in yield stress within a few minutes after mixing [30].

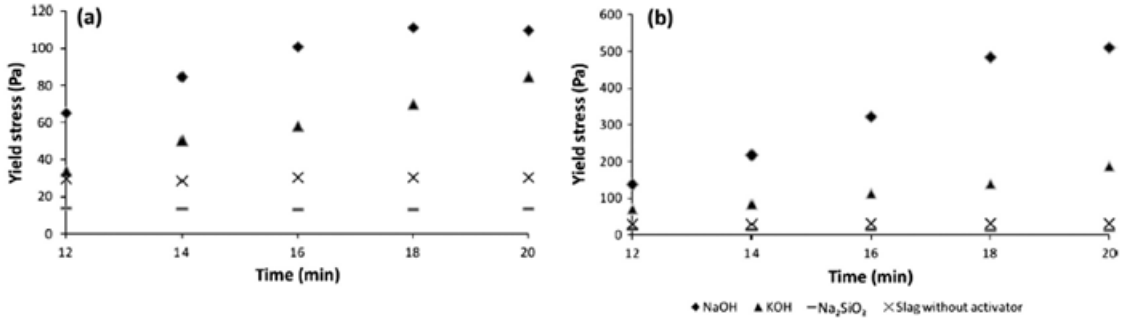

Figure 11: Yield stress of the alkali-activated slag pastes with (a) 2.25 · 10^{-4} and (b) 4.5 · 10^{-4} moles M_2O/g slag, and slag paste without activator, as a function of time after initial mixing [30].

The effect of the alkali hydroxide activator is also confirmed by the fact that the slag pastes without activator showed no evident change in the yield stress. According to Hamada et al., this is due to the fact that the activator action causes inter-particle adhesion and/or dissolution reaction (gelation) [31].

2.8.1 Surface chemistry of GGBFS in water

In order to understand the rheological properties and zeta potential of paste dependent on activator, as well as to analyze the relationship between zeta potential of slag and yield stress meaning, the surface chemistry of slag in water has to be studied.

E. Nägele in his publication, he defined the zeta-potential as the potential of the shear plane between liquid phase and suspended solids [32]. Habbaba et al., measured the zeta potential of three different slag suspensions, with initial results ranging from a negative value to a strongly positive value (Figure 12) [33].

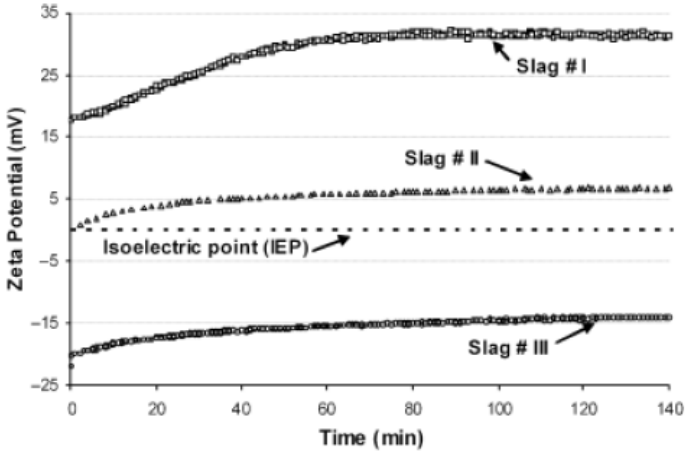

Figure 12: Time-dependent zeta potentials of slag samples dispersed in DI water [33].

It follows that one of the factors influencing the zeta potential of the slag is its chemical composition.

A measurement of the zeta potential over several hours also showed that in different modes, the zeta potential value of any of the samples increased either to a lower or higher value. Such changes may indicate that the components present in the slag tend to dissolve over time. The authors confirm this by observing that in the same experiment, in order to study the dependence of the zeta potential change with time, a change in pH could also be observed.

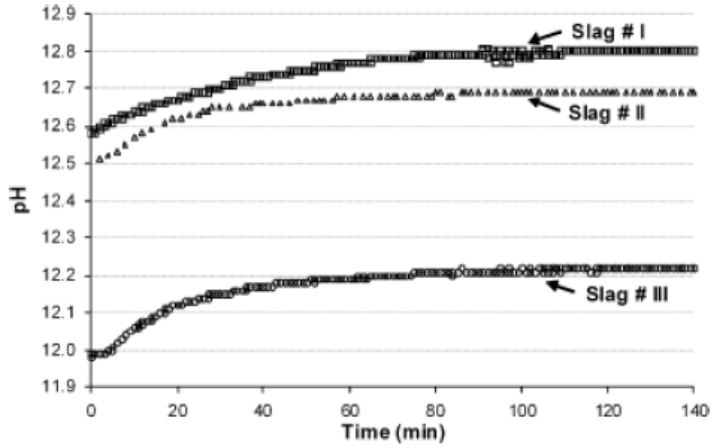

Figure 13: Time-dependent pH values of slag samples dispersed in DI water [33].

Differences in pH values between slag samples can be explained by differences in the concentration of alkaline and alkaline-earth Ca^{2+}, Na^{+} and K^{+} cations. The content of such cations can be caused by partial dissolution of the corresponding oxides which are initially contained in one or another sample of slag. Thus, the slag paste containing the greatest amount of alkaline and alkaline-earth cations will develop the highest pH. Correspondingly, the sample containing the least amount of Ca^{2+} and Na^{+} will exhibit a lower pH value. This dependence is expressed by the graph in the picture where the development of alkaline and alkaline-earth ions in the slag samples in deionized water can be observed (Figure 14) [33].

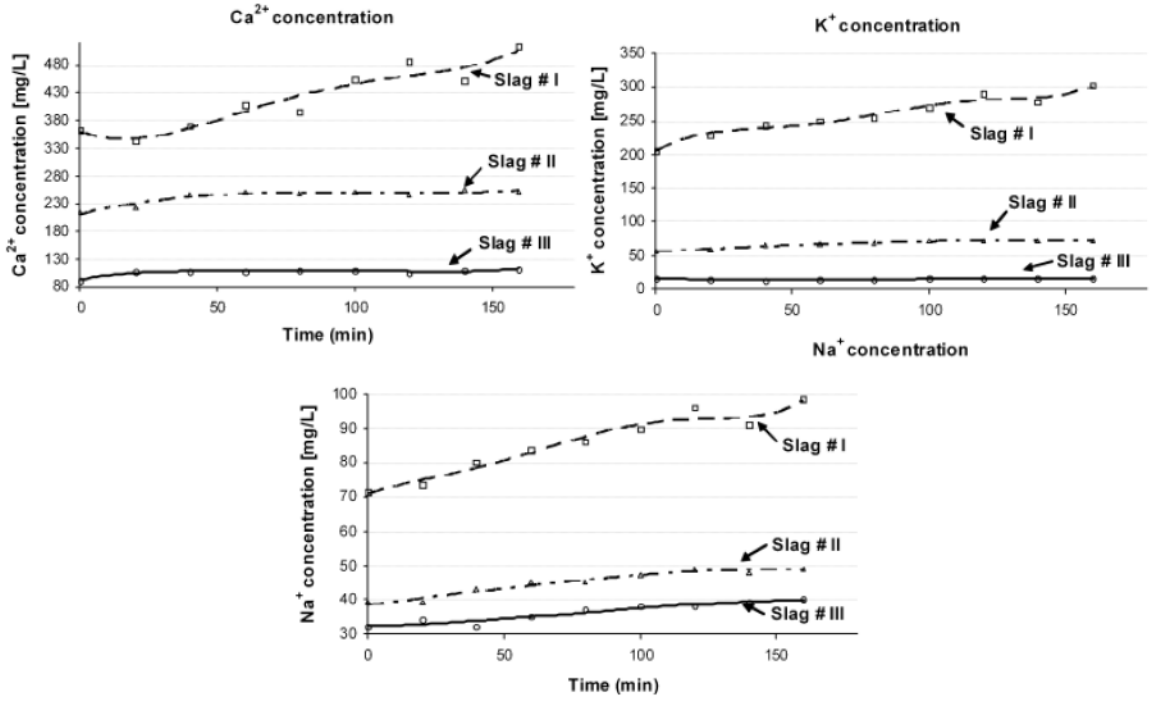

Figure 14: Time-dependent evolution of Ca^{2+}, K^{+}, and Na^{+} concentrations in pore solutions from slag samples suspended in DI water (w/s ratios: 0.55 for slag # I, 0.52 for slag # II, and 0.46 for slag # III) [33].

Kelzenberg et al. claim in their publication that slag in water is not inert, but on the contrary, shows its reactivity [34]. The slag reacts with water to release ions at concentrations that can be observed in cement suspensions with water. The only difference, according to the authors of the study, is that the reactivity of the slag is determined by its chemical composition [34].

Based on the ion concentration, the pH and zeta potential values of the slag samples can be explained. As mentioned earlier, slag samples with a high concentration of alkaline and alkaline-earth ions have a higher pH and show a positive zeta potential value, and vice versa, samples with a low pH value are unable to dissolve enough ions and therefore have a negative zeta potential. These differences may also be due to processes occurring at the pore-solution-slag interface. Plank et al. believe that due to the deprotonation of silanol groups when dispersed in an alkaline solution, all slags have an initially negative zeta potential [35]. Only when alkaline and alkaline earth cations are gradually released into solution, do these cations gradually adsorb to the slag surface with a negative charge.

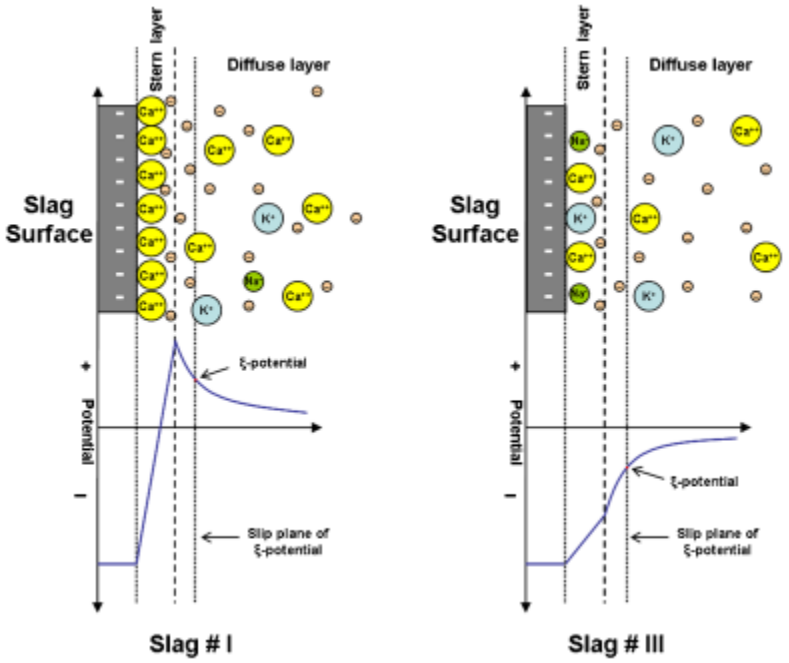

Figure 15: Schematic illustration of the electrochemical double layer that forms at the surfaces of slags # I (left) and # III (right) dispersed in water, and their surface charge as shown by the zeta potential [33].

As can be seen in figure 15, the equilibrium surface of the slag becomes either more negatively charged (slag #3) or positively charged (slag #1). It appears from this that the zeta potential of slag in water is a consequence of adsorption of alkali and alkaline-earth metal ions during dissolution of slag.

2.8.2 An analysis of the rheological properties of the paste based on the type and dosage of activator

Using alkali hydroxide activators to activate slag paste leads to greater yield stress as compared to using alkaline waterglasses activators, according to a study conducted by Kashani et al [30]. A slag pastes without an activator showed no change in yield stress. As a result, it is believed that slag paste activated with alkali hydroxide over a short period of time undergoes changes in yield stress due to the activator causing inter-particle adhesion and/or dissolution/gel formation reactions. The authors of this study state that the paste activated with sodium silicate shows a lower yield than non-activated systems due to the deflocculation activity of particulate matter in many suspensions of alkaline silicate solutions. Kashani suggests that the increase in yield stress of hydroxide-containing pastes may be partly explained by the flocculation effect, and that the dissolution/gel formation process may be similar (or even faster) for silicate-containing pastes [30; 35].

2.8.3 An analysis of zeta potential in relation to activator type and dosage.

Approximately 11.7 pH is observed in the slag suspension in water, according to study conducted by Kashani et al. During this pH change, some silanol groups on the surface are deprotonated, resulting in a negatively charged surface. Based on the results of the experiment it can be seen that the addition of alkaline hydroxides to the slag suspension promotes the transition from a negative to a positive Zeta potential value [30; 36].

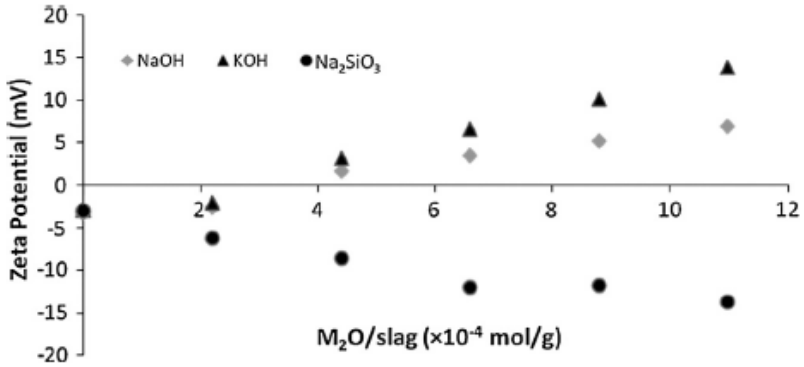

Figure 16: Zeta potential of slag suspensions in water (3 wt.%) after addition of different activator dosages [30].

Partial dissolution of Ca^{2+} from slag particles at high pH and interaction with alkaline cations can significantly affect surface chemistry. A positive value is typically associated with potassium ions, while a negative value is typical for sodium ions. As a well-hydrated ion, Na^{+} binds to water molecules, while K^{+} has a lower charge density and is a poorer hydration state that binds to slag molecules, rather than water molecules [30; 37].

Another effect has also been observed, where sodium silicate added to slag suspension contributes to higher negative zeta potential values, explained by the adsorption of SiO_2 on the slag particles [30]. As stated by Shi et al., this occurs when silicate concentration exceeds Ca^{2+} availability [38]. Hence, zeta potential plays the most important role in the strength of the

electric double layer between particles. Moreover, this force plays a key role in flocculation and dispersion of suspended particles, and its effect is therefore directly related to yield stress [30].

2.8.4 Analysis of the interrelationship between the zeta potential of the slag suspension and the yield stress.

There is a DLVO theory, and its case for oxide suspensions states that there are two basic forces between particles, these are the attractive Van der Waals forces and the repulsive electrostatic forces induced through the formation of a double layer of ions with opposite potential-determining signs. These forces are of key importance in determining a particular interaction between particles. Any factor that strengthens or weakens any type of force will have a direct influence on the structural development of the paste, which will, therefore, in turn, affect the yield stress [39].

It is known that the double layer forces directly depend on the zeta potential, by measuring which it becomes possible to follow changes in the double layer forces. An equation 5 has been developed which clearly demonstrates the relationship between the double layer forces and the yield stress [40]:

$$\tau_y = K_{struc}[F_{VDW} - F_{EDL}];\ (F_{EDL} \sim \zeta^2) \qquad \text{Eq. (5)}$$

Where τ_Y: yield stress, K_{struc}: slag structural parameter, F_{VDW}: van der Waals force, F_{EDL}: electric double layer forces, ζ: zeta potential.

Based on this equation, when the zeta potential is zero, the yield stress will be maximum. When the zeta potential increases, the repulsive forces of the double layer between the particles increase along with it, resulting in a decrease of inter-particle forces and a respectively lower yield stress.

It was found that when a large number of weakly soluble ions are adsorbed on the particle surface, zeta potential together with the yield stress are increased, compared to when the zeta potential is zero. Franks et al., state that in order to minimize free energy, the ions take positions between the surfaces of neighboring particles, which in turn contributes to the formation of the attraction force [41]. The author argues that this strong coupling between the particles, in a timely manner, leads to flocculation and may be the cause of increased yield stress.

A similar trend where an increase in zeta potential can be observed with the addition of an activator is reported by Kashani et al. Figure 17 shows that with the addition of sodium waterglass an increase in zeta potential can be observed, and as a consequence a decrease in the yield stress of the paste due to an increase in the repulsive forces of the double layer [30]. The authors point out that although increasing the Na_2SiO_3 concentration increases the zeta potential it may also lead to an increase in the yield strength. This may state that, although the force of the electric double layer increases with increasing concentration of the additive, this force is no longer only repulsive; on the contrary, it shows certain signs of an attraction force.

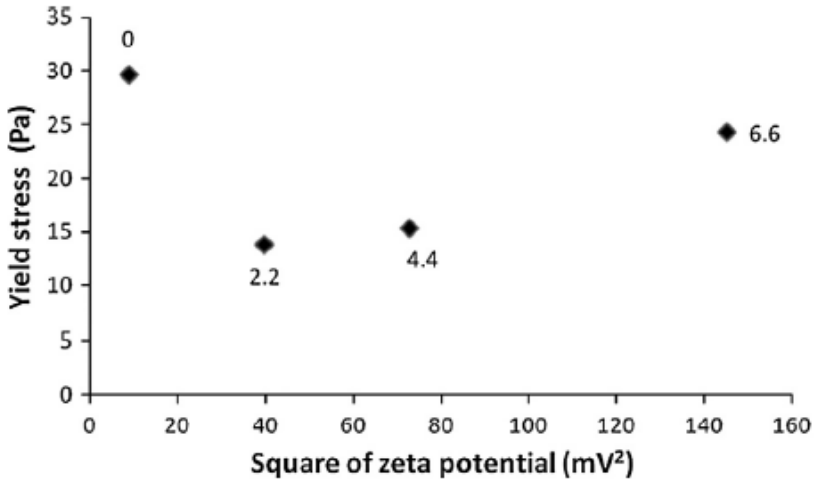

Figure 17: Relationship between the square of zeta potential of slag suspensions at 0, 2.2, 4.4, and 6.6 x 10^{-4} mole Na_2O/g slag (as marked on each point) and the yield stress of sodium silicate-activated slag paste at w/c = 0.45 [30].

Labbez et al. explain this by the fact that silicate anions are adsorbed on the slag surface, in areas that carry a positive charge due to Na^+ and Ca^{2+} cations and that screen the silanol groups of the slag [36]. This can be the cause of the repulsive forces of the electrical double layer between the slag particles. The resulting repulsive forces also contribute to the separation of the particles, as evidenced by the increase of the zeta potential at low pH. If the Na_2SiO_3 addition is increased, an increase of negative zeta potential can be observed, but according to Kashani et al., it also increases the pH, which promotes slag dissolution and the release of various cations, like Ca^{2+} Mg^{2+} into the solution [30].

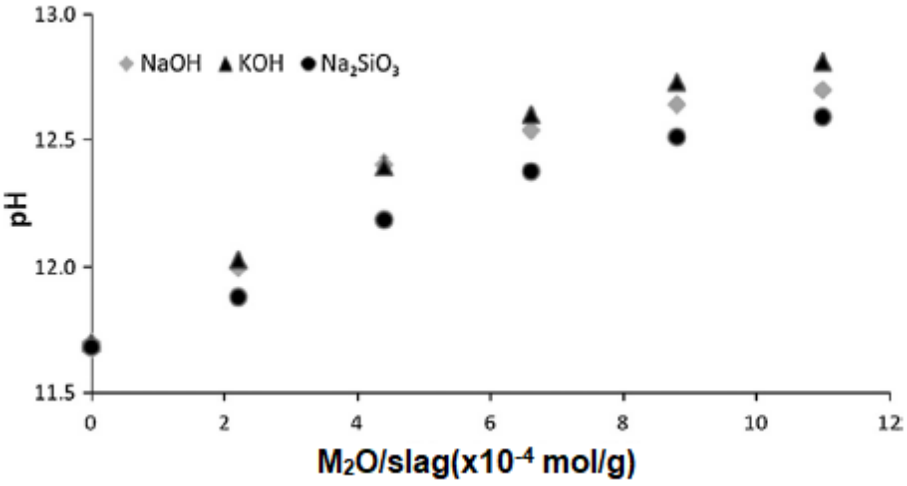

Figure 18: Measured pH of 3 wt.% slag suspension in water immediately after addition of different activator dosages [30].

However, the liquid phase of the dissolved slag can quickly become oversaturated, which can lead to gel formation. The figure shows that the Ca^{2+} and Mg^{2+} cations are more likely to adsorb on the silanol cations than on Na^+ and K^+ due to their double charges.

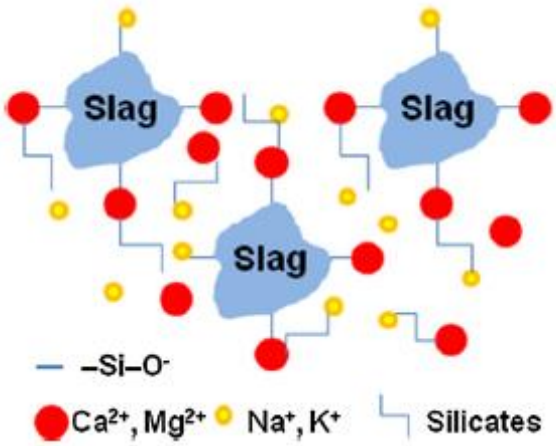

Figure 19: This schematic illustrates electrostatic inter-particle forces at a high concentration of sodium silicate in a slag paste [30].

Due to the fact that Ca^{2+} and Mg^{2+} are adsorbed on silanol groups, electrostatic bonds can form between silanol groups on different slag particles.

The opposite situation is observed for the slag-activated by alkali hydroxide. It is known that the increase of zeta potential is an indication of the repulsive forces of the double layer, which eventually facilitates to the decrease of yield stress. However, in determining changes in yield stress, rapid dissolution of slag is a more significant factor. Based on that, it is dissolution that causes the most prominent rheological changes in alkali-activated materials [30; 31; 32].

3 EXPERIMENTAL PART

This chapter describes the procedures, methods, materials, and equipment used to conduct the experimental component of this thesis. All experiments and measurements were carried out under laboratory conditions (25 ºC).

3.1 GGBFS composition

Ground granulated blast furnace slag was used as a precursor. The grinding fineness according to the Blaine method was approximately 400 m^2/kg. Median particle size of slag was 11.99 μm. The phase composition of the granulated blast furnace slag obtained by the X-ray Powder Diffraction (XRD) method is shown in table 2.

Table 2: Phase composition of ground granulated blast furnace slag used in (%).

Akermanite	Quartz	Calcite	Merwinite	Amorphous phase
20	2.7	6.7	0.38	70

The chemical composition of the granulated blast furnace slag obtained using the X-ray fluorescence (XRF) method is shown in table 3.

Table 3: Chemical composition of the granulated blast furnace slag used in (%).

MgO	Al_2O_3	SiO_2	SO_3	K_2O	CaO	TiO_2	Mn_2O_3	Fe_2O_3	SrO	ZrO_2	BaO
8.64	8.15	39.80	1.37	1.19	37.35	0.30	0.89	0.74	0.06	0.02	0.12

3.2 Alkaline activators

For slag activation, alkaline solutions of hydroxides, silicates and sodium and potassium carbonates were used. The starting alkaline activators used were sodium waterglass solutions with silicate modulus Ms = 1.89 by Vodní sklo a.s., potassium waterglass with silicate modulus, 3.16 (SChem a.s.), 50% sodium and potassium hydroxide solutions by Carl Roth GmbH, distributed by P-LAB, a.s., and sodium and potassium carbonate solutions by Lach-Ner, s.r.o. The chemical composition of these activators is given in the table 4. It is important to clarify that when reference is made to sample concentration, the concentration of alkali ions in the sample is meant.

In order to reduce and simplify the work on the experiment and data processing, it was decided to abbreviate the samples as follows:

SWG - Sodium waterglass
PWG - Potassium waterglass
PH - Potassium hydroxide
SH - Sodium hydroxide
SC - Sodium carbonate
PC - Potassium carbonate

Table 4: Composition of alkaline activators used in (%).

	SWG 1.89	PWG 3.14	NaOH 50%	KOH 50%
Na_2O	16.94	0	38.38	0
K_2O	0	10.67	0	41.65
SiO_2	30.98	21.54	0	0
Dry matter	47.92	32.21	38.38	41.65
H_2O	52.08	67.79	61.62	58.35

3.3 Mixture preparation

Thirty-seven compositions of alkali-activated slag paste samples were prepared by alkaline activation of the slag with an appropriate activator. In addition, samples of a mixture of slag and water were prepared as a reference.

The weight of the components was chosen to be sufficient to achieve the intended purpose, to ensure sufficient homogenization and to avoid any undesirable over-abundance of material. The smallest amount of slag was targeted at 144.05 g, which was sufficient for the rheological test. Typically, 100 cm^3 of the paste was prepared (see table 5).

The activation time, when the GGBFS was add to the activator solution. was considered time 0 (start of mixing). Immediately after, the mixture was mixed thoroughly with a hand mixer.

The sample history, which includes mixing and processing, significantly affects the properties of the paste and the course of hydration, so a precise mixing procedure was developed and followed when each sample was mixed.

The sample was mixed for the first minute at medium mixer speed, then for thirty seconds at maximum speed. The next half minute in the beaker containing the sample was spent manually separating the sample mixture from the walls of the beaker. Finally, the sample was mixed with the mixer at maximum speed for another minute to achieve greater dispersion. In total the mixing process took exactly three minutes. Once the mixing procedure was completed, the sample was poured into a rheometer or to the cone for mini-slump test.

Table 5: Weights for 100 cm3 of GGBFS pastes using 144.05 g slag, slag volume fraction in paste 0.50 used (in g).

Alkali concentration (mol/dm^3)	1	2.5	4	5	7.5	9	9.953	10	12.5	15
SWG	53.44	58.52	63.39	66.52	73.92	0	80.61	0	0	0
PWG	53.69	59.19	64.47	67.88	76	80.59	0	0	0	0
SH	52.01	54.83	57.51	59.21	63.17	0	0	66.72	69.84	72.55
PH	52.26	55.58	58.76	60.80	65.60	0	0	69.99	73.98	0
SC	52.44	56.05	59.38	61.44	0	0	0	0	0	0
PC	52.75	56.8	60.66	63.14	68.98	0	0	73.30	0	0

3.4 Mini-slump test

From the outset, measurements were made of the flowability of prepared alkali-activated slag paste samples using a metal cone. The measurements were carried out in such a way that a thin layer of silicone oil was applied in small strokes to the inside of the metal cone. The cone was then placed on the surface and gradually filled to the edge with each of the prepared slag pastes, the excess was removed with a special spatula. Five minutes from the start of mixing the cone was gently lifted and the resulting spread diameter was measured by placing metal bars on the edges of the poured slag paste and using a ruler to measure the area of the resulting spill. Each sample of activated slag paste, together with the paste mixed with water, was measured several times to ensure reproducible results.

The mini-slump test was performed using a cone geometry shown in Figure 20, with 57 mm height, 19 mm top diameter and 38 mm bottom diameter, where top and bottom diameters are inner sizes of the cone.

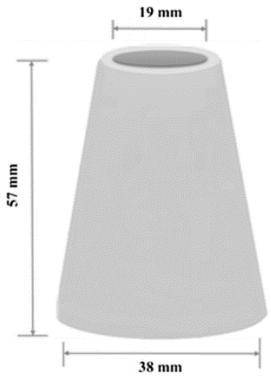

Figure 20: Schematic diagram of mini-slump test cone geometry.

3.5 Methods and equipment used

The Discovery HR-2 hybrid rheometer from TA-Instruments was used to observe the development of viscoelastic properties and time-dependent processes in alkali-activated slag pastes. The prepared pastes were measured on the rheometer using a 20mm diameter vane concentric cylinder with six blades at the cup-vane assembly. Rheological measurements were taken five minutes from the moment the mixing started.

Although different volume fractions were tested at the beginning of the experiment, in this work alkali-activated pastes were calculated to have a slag volume fraction of 0.50.

The sample was dosed with a small double-sided spatula. After stirring the paste was poured into a measuring vessel, geometry was launched, and a program was initiated to determine the rheogram of the prepared pastes.

In order to find the linear viscoelastic region of the mixture, amplitude sweeps were measured in strain controlled and stress-controlled modes at a constant angular frequency of 10 rad/s. These measurements were performed within the specified range of shear strain. For the strain-controlled test, the range was set from $5 \cdot 10^{-4}$ % to 500 %, and for the stress-controlled test, the range was set from 0.05 Pa to 500 Pa. Before the measurement, the soak time parameter was also initiated, which means a certain time, in this work it was 10 seconds, during which the sample had to settle and warm up to 25 ºC.

The information obtained was processed using Trios software. The results of the amplitude sweeps are presented as a diagram are shown in Figure 21, where strain (or shear stress) is plotted on the x-axis, and storage modulus G' and loss modulus G" are plotted on the y-axis, both logarithmic scales.

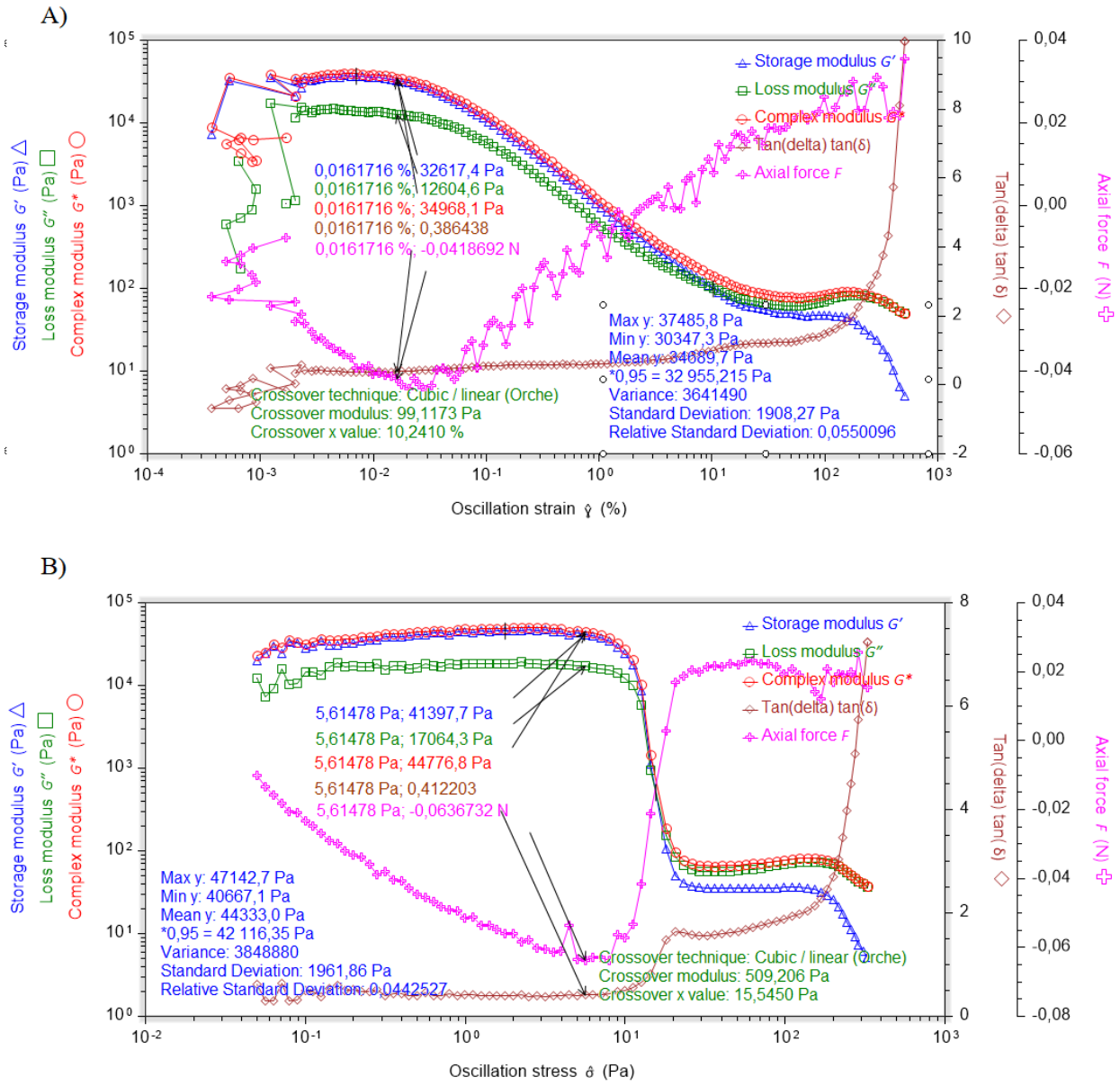

Figure 21:Results of two amplitude sweeps of potassium hydroxide-activated paste with a potassium ion concentration of 1 mol/dm^3: A) strain-controlled test; B) stress-controlled test.

First, the LVE region was determined, which indicated the test region without destroying the structure of the sample. The LVE was defined by using the curve of the G′ function, which shows a constant value (plateau). The linearity limit was determined using a ruler and was calculated from the strain γ_L in percent (in the case of the stress-controlled test, the linearity limit was calculated from the stress in pascals). The tolerable deviation range for G′ around the plateau value was ±5%. G′, G″, G*, and tan(δ) values in the LVE region were then evaluated on the corresponding curves. The yield point and flow point were also determined using

amplitude sweeps (regardless of whether a controlled stress test or a controlled strain test was performed). The values were determined on a diagram in the region between yield point and flow point. The data of the obtained parameters were stored in an appropriate table, which was then used to plot the development of the rheological parameters of the activated paste depending on the activator and its concentration.

3.6 Zeta potential

The zeta potential of blast furnace slag was also studied using the Zetasizer Nano ZS by Malvern Panalytical. This device is used to measure the particle size of disperse systems up to a few micrometers in diameter using the dynamic light scattering (DLS) method.

The samples for the measurements were prepared in a similar way as in the rheological measurements with the only difference being that the samples for the zeta potential measurements were prepared in a smaller set. Also, because of the lower ratio, mixing was not done with a mixer, but by hand. The time period was the same as in the rheological measurements. Once the sample was ready, it was thoroughly mixed with distilled water and transferred to a container with volume of one liter. To avoid sedimentation, the sample was thoroughly stirred with water. Then, using an injector, the sample was dosed into a special column, in which the zeta potential of the sample was measured. This procedure was performed three times for one sample. A total of 38 samples were measured, including a sample of slag paste with water.

4 RESULTS AND DISCUSSIONS

4.1 Mini slump test

First, it was determined how the prepared pastes spread under its own weight after lifting the cone, depending on the activator used.

As it can be seen in Figure 22, suspension of slag in water reached relatively low spread diameter of about 50 mm. Further, the spread diameter was strongly dependent on the used activator as well its concentration.

At an initial concentration of 1 mol/dm^3, samples activated by carbonate activators together with potassium waterglass spread over an area in diameter of 60 to 75 mm. Sodium waterglass together with sodium hydroxide did not exceed 50 mm in diameter at the initial dosage. Immediately it can be observed how the paste activated with potassium waterglass shows the highest result, where at only 4 mol/dm^3 concentration the sample reached an area of 125 mm in diameter, but as the concentration of alkaline ions in the activator increased, the diameter of the spreading paste narrowed to 109.5 mm. It is noticeable that as the concentration of sodium ions in the sodium waterglass activator increased, the diameter of the paste gradually increased, approaching 99 mm. However, at a concentration of 9 mol/dm^3, the resulting sample was already unmeasurable, presumably due to the high viscosity of the activation solution. It could lead to the fact that when the activation solution mixed with slag, the paste is not liquid enough.

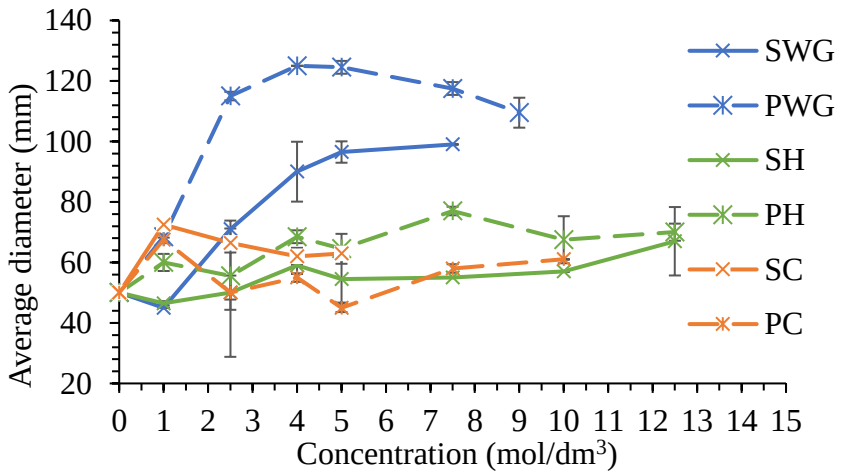

Figure 22: Spread diameter of a paste with slag and activator dose mixed by using the high shear mixer.

The spread diameter of the sodium hydroxide-activated paste increased with increasing sodium ion concentration in the activator tend to increase across the full concentration range. The same trend, yet more scattered, was observed also for potassium hydroxide-activated slag. In general, it can be observed that potassium-activated samples flow better than sodium-activated samples.

Based on the results shown in Figure 22, one can observe the tendency of the pastes activated by carbonate activators to increase the spread. It is worth to mention that pastes activated with sodium carbonate show a greater tendency to increase the spread than potassium carbonate. Unfortunately, the values are rather scattered, and it is impossible to make more detailed conclusions without further studies.

4.2 Rheological behavior of alkali-activated slag

4.2.1 Strain controlled test

The main objective of this thesis was to carry out oscillatory measurements to assess the influence of the activator nature and concentration on the rheological behavior of alkali-activated slag pastes. As mentioned, both strain and stress-controlled tests were used. This section summarizes the results obtained using the former type of the test.

The parameters corresponding to the LVE region determined using the approach described in section 3.5 are summarized in Figure 23–27.

Thus, comparing the parameters obtained as a result of strain-controlled amplitude sweeps (Figure 23), one can observe how the value of the oscillation strain parameter changes with increasing concentration. The hydroxide-activated pastes strain first slightly decreases with increasing concentration, and then after 5 mol/dm^3 strain begins to increase. The tendency of silicate-activated pastes is not clear because of the values scatter. It looks like for sodium waterglass-activated slag pastes the strain tends to grow, while samples with potassium waterglass activator represent a decrease in strain. The same behavior can be observed with carbonate-activated samples. Generally, it seems that the cation influence on strain is negligible within the measurement uncertainty.

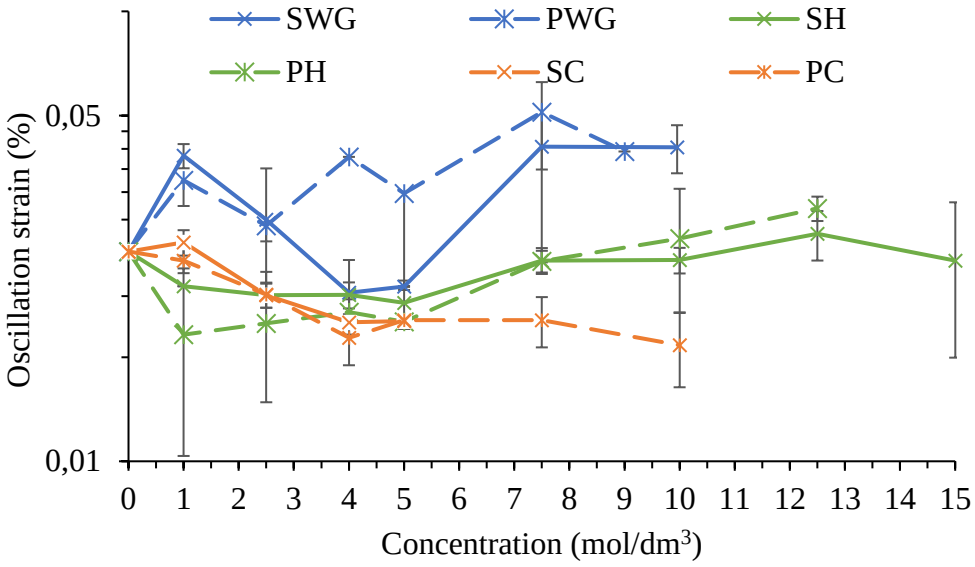

Figure 23: Evolution of oscillation strain parameter of GGBFS paste activated at different activator concentrations.

The evolution of elastic modulus with increasing concentration of the used activators is given in **Ошибка! Источник ссылки не найден.**. In the sample of activated potassium waterglass, a consistent decrease in the storage modulus can be observed with increasing activator dosage. Samples activated by carbonate activators show the same behavior (by trend); as the concentration of sodium or potassium ions in the activator increases, the parameter values decrease, but reach about one order of magnitude higher values compared to the waterglasses.

However, in hydroxide-activated samples, it seems that use of low concentrated hydroxides leads to the increase in storage modulus of the tested pastes. Gradual decrease in storage modulus can be observed, when the concentrations exceed 1–2.5 mol/dm^3. Sodium hydroxide-

activated pastes show threshold concentration of 7.5 mol/dm^3 above which storage modulus starts to significantly increase.

Similar observations regarding this issue can be found in a literature. According to studies conducted in this area [20; 42], there is a critical value of NaOH concentration, at which the rheological characteristics change. In Figure 24, it can be seen that the concentration of 7.5 mol/dm^3 is the critical value, below which the yield stress and storage modulus (G′) of the paste decrease, and above which these parameters increase with raising concentration. Hydroxide ions play the role of a chemical agent which stimulates the dissolution of solid aluminosilicates, and Na^+ ions are required to place in the voids of tetrahedrons to compensate for the electrical charge due to Si^{4+} substitution by Al^{3+}. Consequently, ion concentration affects the competition between dissolution and polycondensation kinetics, thereby affecting viscoelasticity.

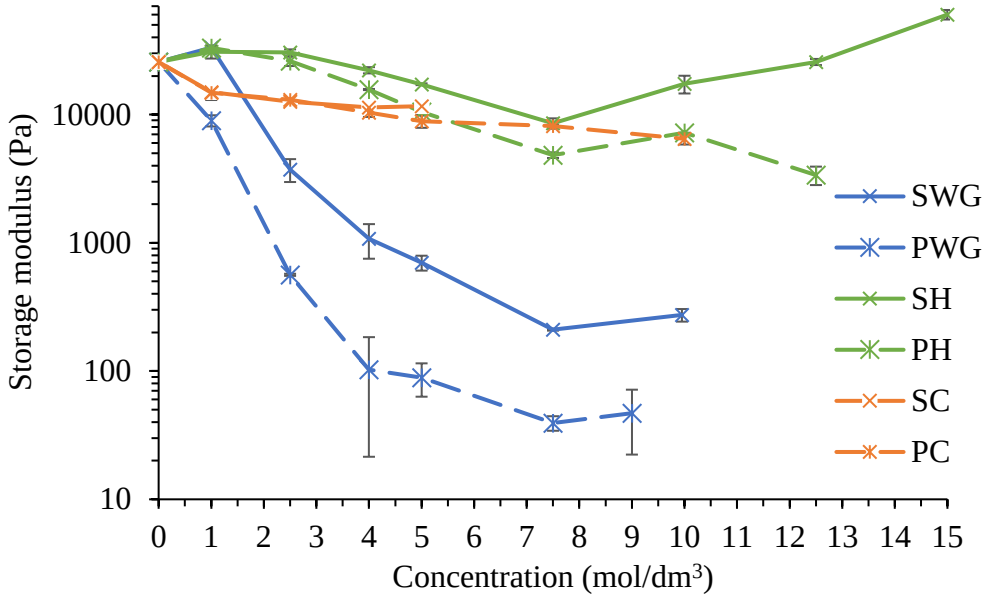

Figure 24:Evolution of storage modulus of GGBFS paste activated at different activator concentrations.

Figure 25 shows the evolution of stress of GGBFS paste activated at different activator concentrations. The trends are similar to those already described within other parameters corresponding to LVE region, as the stress, strain and (complex) modulus relate to each other.

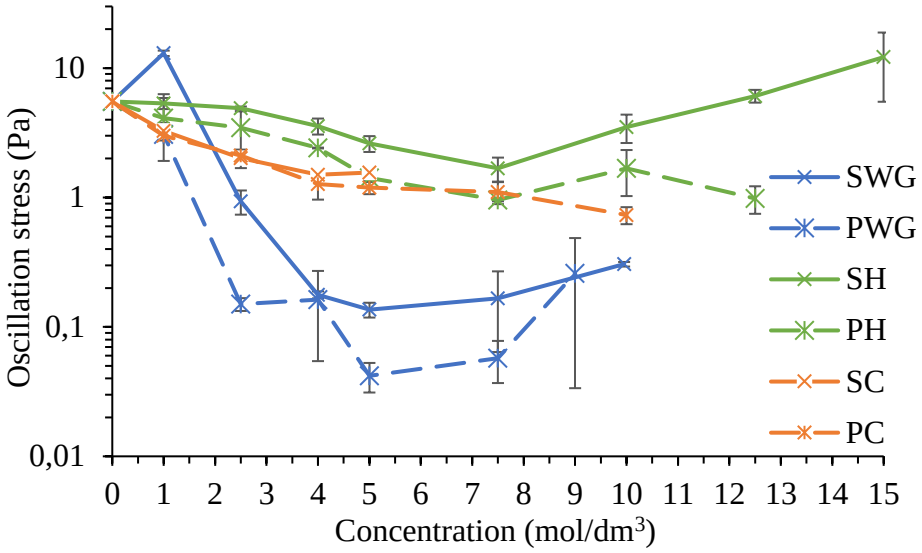

Figure 25: Evolution of stress calculated by TRIOS software of GGBFS paste activated at different activator concentrations

The Figure 26 shows the tangent of the loss angle, so called loss factor. It represents the ratio between the energy dissipated as heat and the stored energy. The effect of the activator on the loss factor also differs for different activators. First of all, a different behavior of samples activated by silicate activators compared to other activators can be seen. Increasing concentration of both silicates results in significant increase in loss factor, especially for concentrations above 2.5–4 mol/dm^3. This is associated with the change of the rheological nature of the pastes from solid-like to liquid-like and reach the values of loss factor of 2.5–3 for the highest concentrations. The more rapid change of loss factor can be observed for potassium-based silicate compared to sodium one, which is in accordance with the previously discussed results related to the nature of alkali cations as well as to the rheological properties of these solution alone, as the potassium silicates has much lower viscosity compared to the sodium silicates of the same concentration [30]. The observed effect of silicates on rheology is probably related to the plasticizing effect of silicates that adsorbs onto the slag particles surface, which leads to the great reduction of zeta potential and thus increase the repulsive forces [30].

Unlike silicates, both hydroxides and carbonates affected the loss factor in a very limited extent. Both sodium carbonate and sodium hydroxide rather decrease the loss factor with their increasing concentration, although low concentrations of sodium hydroxide reached slightly higher loss factor values compared to slag in water.

The sample activated with potassium hydroxide shows very similar behavior, but once the concentration of potassium ions reaches 7.5 mol/dm^3, the value of the loss factor begins to increase dramatically, up to the highest dosage.

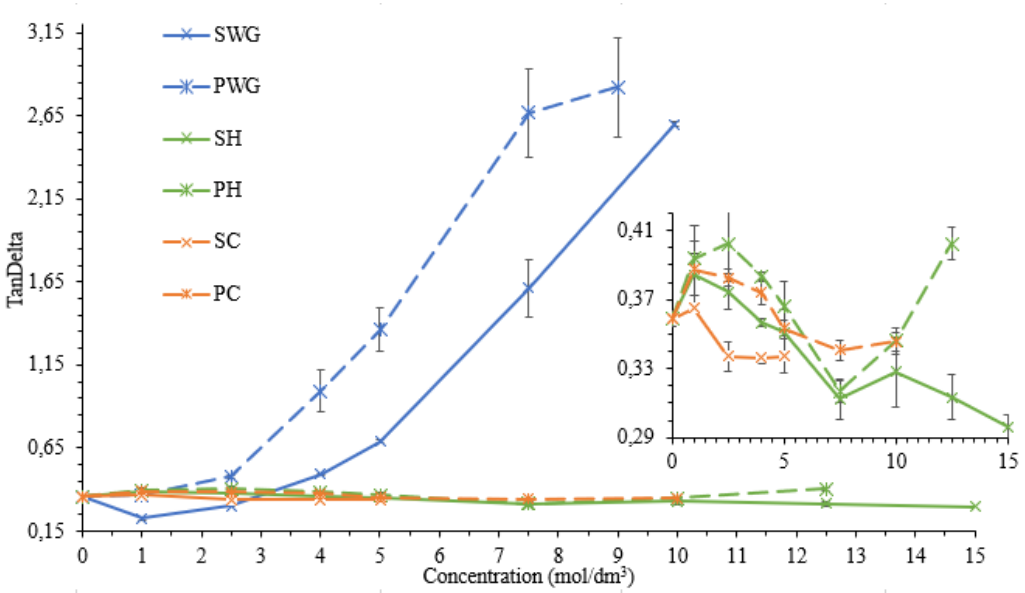

Figure 26: General evolution of tangent delta of GGBFS paste activated at different activator concentrations with inside closure look at 0.29 – 0.42 tangent delta value.

So far, the parameters describing the start of the disruption of the pastes' structure were assessed. However, another important parameter roughly corresponding to the yield stress determined using flow curves is the flow point observable on the amplitude sweep curves, where the storage modulus prevails over the loss modulus. Therefore, the flow point can be determined as the crossover of these moduli.

The effect on crossover stress shown in Figure 27 has very similar trends to the previous parameters. The crossover stress of slag pastes peaks at the initial dosing with sodium waterglass activator. The explanation for the initial increase in oscillation stress is not clear, but possibly, the lowest concentration of sodium silicates is not sufficient to reach the plasticizing effect.

With increasing concentration of sodium ions in the activator, crossover stress decreases. Crossover stress of potassium waterglass-activated paste decreases starting with the first activator dose. For both silicates, crossover stress is shown only for their lower concentrations, as higher concentrations shifted the values of loss factor above one since the beginning of the measurement, so the modulus crossover was not observed.

Similar to the LVE region limit, threshold concentration of sodium hydroxide of 7.5 mol/dm^3 above which crossover stress starts to dramatically increase can be observed. In this case, however, the increase is much higher compared to that for the LVE region limit which suggest that concentration of NaOH has larger impact on the flow point compared to the yield point. The sample activated with potassium hydroxide shows a continuous decrease in crossover stress over the whole concentration range with one exception of 10 mol/dm^3. In contrast to sodium hydroxide, there are much smaller differences between the effect of concentration on the yield point and flow point.

The sample activated with sodium carbonate shows a decrease in the crossover stress with increasing concentration of sodium ions up to a concentration of 2.5–4 mol/dm^3, after which a slight increase in the parameter value can be observed, but the differences are very low. The

sample activated with potassium carbonate shows a gradual decrease in crossover stress with higher concentration of potassium ions in the activator, i.e., similar trend as for potassium hydroxide can be observed. Interestingly, increasing concentrations of carbonates affect more yield point than flow point.

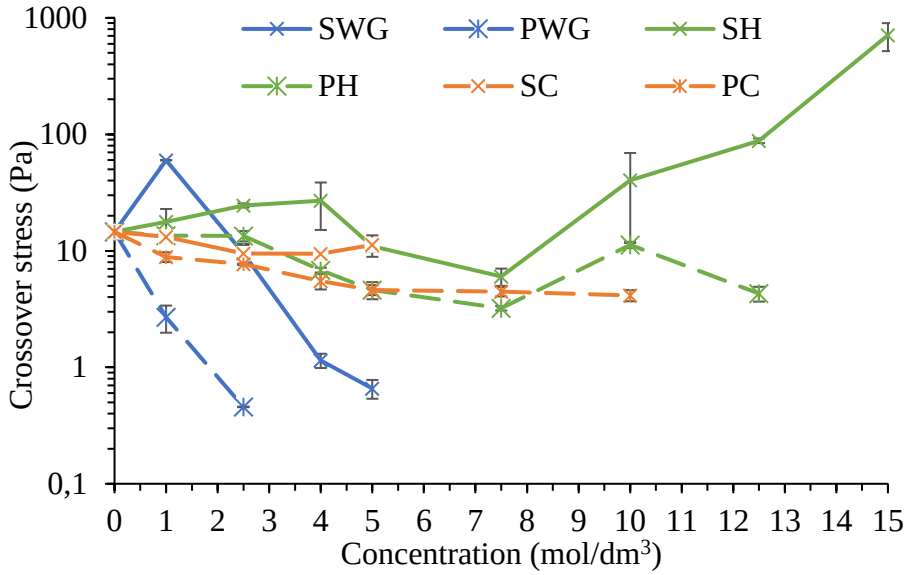

Figure 27: Evolution of crossover stress parameter of GGBFS paste activated at different activator concentrations.

4.2.2 Stress controlled test

Thus, comparing the parameters obtained from the stress-controlled amplitude sweeps test, very similar trends can be noticed. Comparing the results obtained from stress-controlled amplitude sweeps shown in Figure 28, one can observe how oscillation strain changes with increasing concentration. The hydroxide-activated pastes behave in almost identical way, when after slight decrease with increasing concentration, after 5 mol/dm^3 strain starts to grow. The tendency of silicate-activated paste is clearer compared to the strain-controlled amplitude sweep test. Once can notice that after quiet significant oscillation stress growth, when concentration 5–7.5 mol/dm^3 reached, the strain decreases. Carbonate-activated pastes show quiet similar tendencies. Then again, it looks like the cation effect is insignificant within the test mode.

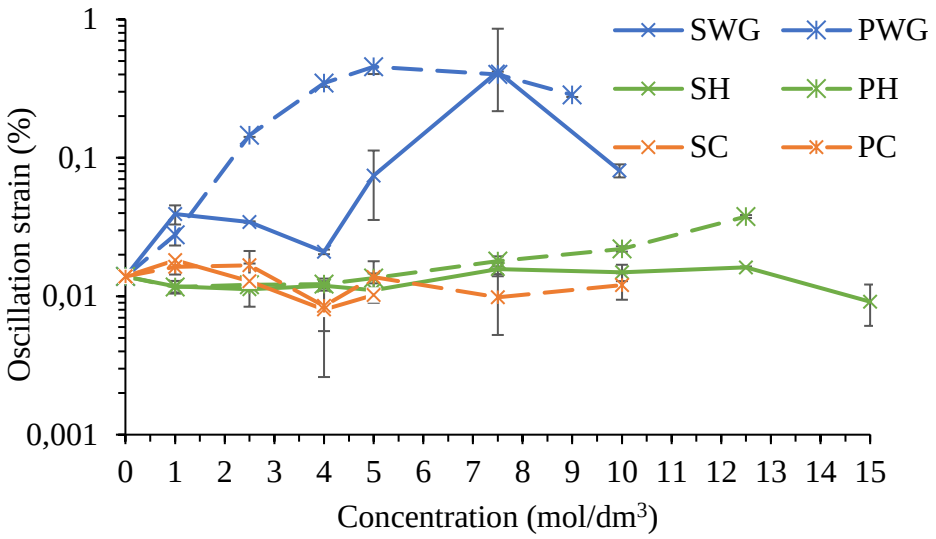

Figure 28: Evolution of strain calculated by TRIOS software of GGBFS paste activated with different activator concentrations

The evolution of elastic modulus obtained via stress-controlled test in Figure 29, shows almost identical trends. Storage modulus of silicate activated pastes decrease with increasing concentration. Pastes activated by carbonate activators and hydroxide activators show the same trend as in previous test.

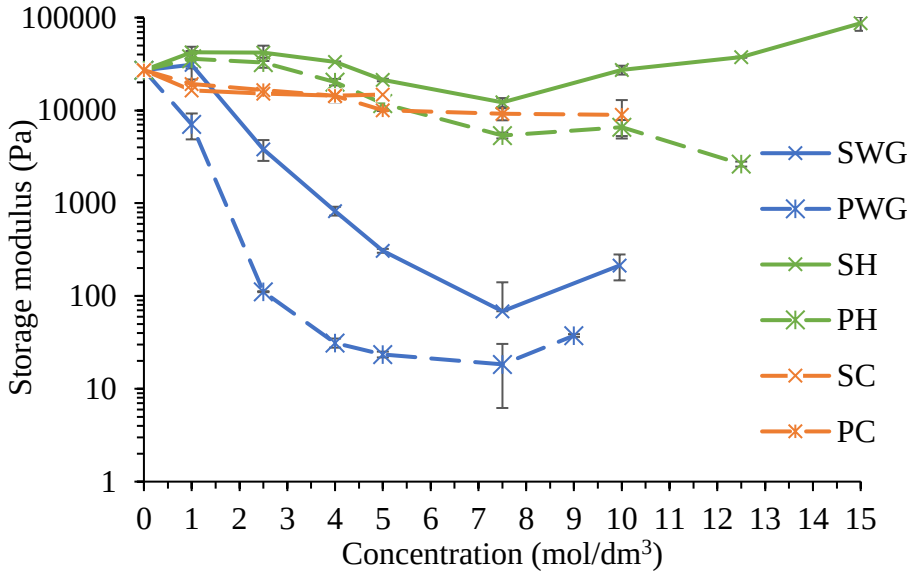

Figure 29: Evolution of storage modulus of GGBFS paste activated with different activator concentrations.

Oscillation stress trends shown in Figure 30 are almost analogous to those obtained with strain-controlled test.

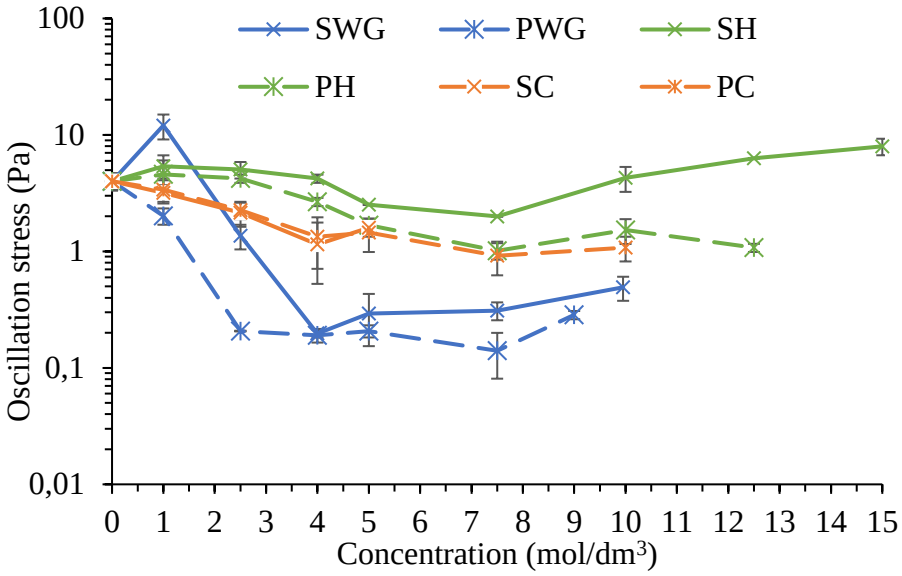

Figure 30: Evolution of oscillation stress of GGBFS paste activated with different activator concentrations.

Again, loss factor shown in Figure 31 shows identical tendencies as those obtained with strain-controlled test. With increasing concentration of silicate activators, a notable growth of loss factor. Both hydroxides and carbonates decrease with increasing concentration, but sodium hydroxide-activated slag shown unsignificant growth compared to slag paste in water.

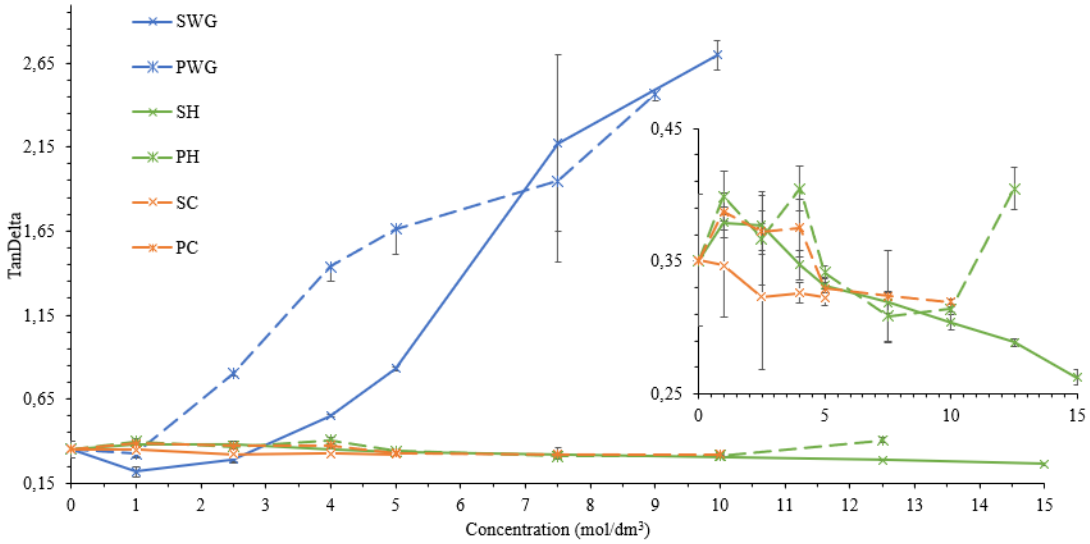

Figure 31: General evolution of tangent delta of GGBFS paste activated at different activator concentrations with inside closure look at 0.25 – 0.45 tangent delta value.

As can be seen in Figure 32, crossover stress shows very similar tendencies as the one achieved with the previous test. Similar peak of sodium silicate-activated paste can be seen at concentration 1 mol/dm^3, but with increasing concentration of alkaline ions crossover stress decreases. Unlike the previous result obtained with strain-controlled test, the threshold concentration of sodium hydroxide-activated slag in stress-controlled test is 5 mol/dm^3, above which the crossover stress starts to significantly grow, though crossover stress of slag paste activated with potassium hydroxide decreases. Carbonate-activated samples behave in identical

way compared to the previous test. Crossover stress of sodium carbonate-activated slag after minor decrease with increasing concentration shows slight increase, but with no significant difference, which is similar trend with potassium hydroxide-activated slag. It also seems that potassium carbonate-activated paste after gradual decrease in crossover stress with increasing concentration shows very negligible growth.

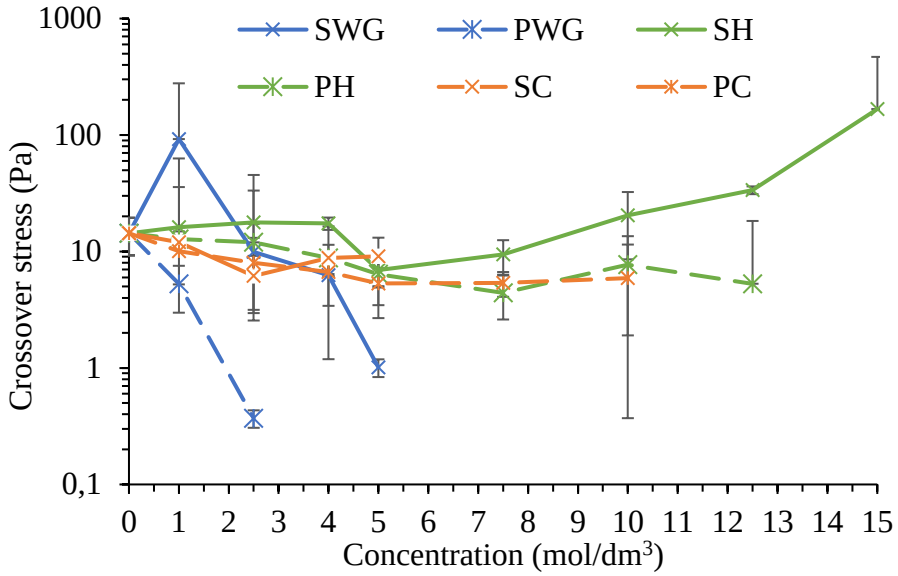

Figure 32: Evolution of crossover stress parameter of GGBFS paste activated with different activator concentrations.

4.3 Surface chemistry measurements

In this work, an attempt was made to establish the relationship between the zeta potential and other parameters of the tested samples. The values of the zeta potential of the slag are shown in Figure 33.

4.3.1 Zeta potential

According to the literature GGBFS in water has a basic pH, which in turn may cause a negatively charged surface, since at this pH the silanol groups on the wetted particle surface tend to deprotonate, hence the slag suspension in water usually exhibits negative zeta potential. This is also the case of the slag used in this work, as can be seen from Figure 33.

When alkaline hydroxides are added to the slag suspension, zeta potential values become less negative and at high concentrations the transition from a negative to a positive value occurs. The same trend has been already published by Kashani et al., where, however, the trend in zeta potential starter at less negative values even for slag in water and thus early overcome the isoelectric point [30]. In contrast to the present study, Kashani observed noticeably higher zeta potential values for KOH than for NaOH, which they attributed to the fact that of the two alkaline ions, Na^+ is the more hydrated ion, which means that it exhibits a greater tendency to

bind to water molecules which reduces its adsorption onto the slag particles. At the same time, K^+ is a larger and less hydrated ion [30; 44].

As can be seen from Figure 33, for samples activated by silicate activators, and sodium carbonate, with their increasing concentration up to 7.5 mol/dm^3, the value of zeta potential drops to the more negative values. The highest changes occur at the lowest concentrations. At very high concentration, the values of zeta potential of potassium carbonate as well as both silicates begin to increase.

Comparing the results from the zeta potential measurement and rheological investigations, one can observe that the zeta potential for hydroxides approaching zero suggest adverse effect of increasing concentration on the rheology of alkali-activated slag pastes. This, however, contradicts the rheological results obtained from both, mini-slump test and amplitude sweep measurements, where increasing hydroxide concentration up to 7.5 mol/dm3 resulted in improved fluidity (in terms of increasing spread diameter or decreasing yield point and flow point). Possible explanation could be the inevitable dilution of the pastes for zeta potential measurement, which could shift the obtained zeta potential to the more negative values that originally were in the pastes prior their dilution. If the values started less negative, isoelectric point would be transited for much lower alkali concentrations and thus further increase in concentration would reduce the extent of attractive forces, so the paste structure is weakened.

For silicate activators, plasticizing effect via adsorption of silicates onto the slag particles was confirmed by zeta potential measurements, indicated by its significantly negative values. It is interesting, that although carbonates-activated pastes exhibited only slightly less negative values of the zeta potential, there were much less fluid compared to the activation with silicates. Possible explanation can be the size of anionic groups of both activators, as it can be expected that silicate species, especially the oligomers or polymers, act on larger distance compared to the carbonate anions.

At the highest concentrations, increasingly plasticizing effect of silicates diminished, which again corresponds with the obtained values of zeta potential. Increase in yield stress at high silicate doses compared to their lower doses was also observed by Kashani et al., although the zeta potential values continued to decrease [30]. They suggested the reason was attractive dipole interactions.

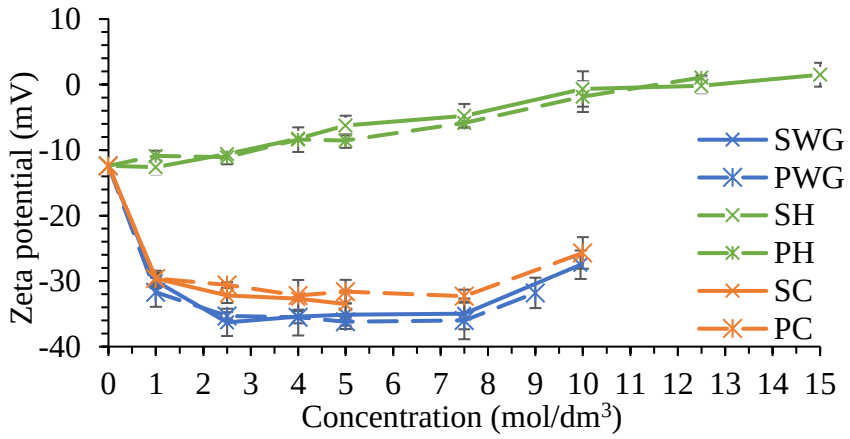

Figure 33: Effect of variation of different alkaline activators on zeta potential of alkali-activated slag samples.

4.4 Conclusion

The purpose of this thesis was to observe the evolution of the viscoelastic parameters of alkali-activated slag mixtures depending on the type of alkaline activator used, using a still relatively non-traditional approach of oscillatory rheology (amplitude sweep tests). The results obtained were compared with zeta-potential results and analyzed.

Based on the results of the experiments performed, it was concluded that the type of activator is the predominant factor influencing the rheological behavior of AAM. In addition, the mechanism of adsorption on the precursor surface can affect the rheological properties of AAM. Sodium-based activators cause higher yield stress than potassium-based activators, which, in turn, can also be explained by differences in the size and solvation of alkaline ions. It is also clear from the experimental results that most activators have a certain concentration value after which the rheological properties of the samples tend to change, which in turn can affect activation. The reason for this phenomenon may be the small Na^+ ions with a higher charge density, which strongly attract and retain their hydration layer of water molecules, whereas K^+ ions exhibit weaker binding to water. In other words, K^+ ions are more likely to bind to negatively charged silicates.

It has also been confirmed that the alkaline hydroxide activator, in this work it was potassium hydroxide, significantly increases the yield stress of AAS, especially noticeably at higher concentrations, possibly because the reactions occur in fresh paste. The reason for this phenomenon may be water consumption, as well as the formation of gel-like reaction products that might introduce new interparticle forces.

GGBFS activated by silicate activators in the case of sodium silicate rather unexpectedly shows a sharp increase in the yield stress, but already with the initial addition of the activator the yield stress decreases compared to non-activated GGBFS, which may be due to plasticizing and deflocculating action of silicate ions. These ions are deposited on the surface of slag particles, thereby increasing the repulsive forces of the double layer and, therefore, reducing the yield stress.

In the future, it may be promising to observe the evolution of viscoelastic parameters during hydration using different activator mixtures prepared from different precursors for a more detailed understanding of the behavior of alkali-activated slag systems.

5 REFERENCES

[1] SHI, Caijun, P. KRIVENKO a D. ROY. *Alkali-activated cements and concretes* [online]. London, 2006. ISBN 04-157-0004-3.

[2] BARSOUM, M., A. GANGULY a G. HUG. Microstructural Evidence of Reconstituted Limestone Blocks in the Great Pyramids of Egypt. *Journal of the American Ceramic Society* [online]. 2006, **89**(12), 3788-3796. ISSN 0002-7820. Dostupné z: doi:10.1111/j.1551-2916.2006.01308.x

[3] *Alkali activated materials: state-of-the-art report, RILEM TC 224-AAM* [online]. Dostupné z: doi:978-94-007-7671-5

[4] KRIVENKO, Pavlo. Why Alkaline Activation – 60 Years of the Theory and Practice of Alkali-Activated Materials. *Journal of Ceramic Science and Technology* [online]. 2017, **2017**(3), 323-334. Dostupné z: doi:10.4416/JCST2017-00042

[5] BONDAR, Dali, C.J. LYNSDALE, Neil B. MILESTONE, N. HASSANI a A.A. RAMEZANIANPOUR. Effect of type, form, and dosage of activators on strength of alkali-activated natural pozzolans. *Cement and Concrete Composites* [online]. 2011, **33**(2), 251-260. ISSN 09589465. Dostupné z: doi:10.1016/j.cemconcomp.2010.10.021

[6] YUAN, B., Q.L. YU a H.J.H. BROUWERS. Time-dependent characterization of Na 2 CO 3 activated slag. *Cement and Concrete Composites* [online]. 2017, **84,** 188-197. ISSN 09589465. Dostupné z: doi:10.1016/j.cemconcomp.2017.09.005

[7] FERNÁNDEZ-JIMÉNEZ, A. a F. PUERTAS. Setting of alkali-activated slag cement. Influence of activator nature. *Advances in Cement Research* [online]. 2001, **13**(3), 115-121. ISSN 0951-7197. Dostupné z: doi:10.1680/adcr.2001.13.3.115

[8] XU, Hua, John PROVIS a Pavlo KRIVENKO. Characterization of Aged Slag Concretes. *American Concrete Institute (ACI)* [online]. 2008, **105,** 131-139. ISSN 0889-325X. Dostupné také z: https://www.concrete.org/publications/acimaterialsjournal.aspx

[9] YUKSEL, Isa, ed. Blast-furnace slag. SIDDIQUE, R. a P. CACHIM. *Waste and Supplementary Cementitious Materials in Concrete* [online]. Woodhead Publishing Series in Civil and Structural Engineering. 2018, s. 361-415.

[10] ÖZBAY, Erdoğan, Mustafa ERDEMIR a Halil İbrahim DURMUş. Utilization and efficiency of ground granulated blast furnace slag on concrete properties – A review. *Construction and Building Materials* [online]. 2016, **105,** 423-434. ISSN 09500618. Dostupné z: doi:10.1016/j.conbuildmat.2015.12.153

[11] MEC, Pavel, Jana BOHÁČOVÁ, Josef KOŇAŘÍK a Petr ZÁVRSKÝ. Alkali Activation of Blast Furnace Slag by Various Types of Activators. *Solid State Phenomena* [online]. 2015, **244,** 94-101. ISSN 1662-9779. Dostupné z: doi:10.4028/www.scientific.net/SSP.244.94

[12] BOUAZIZ, Ahmed, Rabah HAMZAOUI, Sofiane GUESSASMA, Ridha LAKHAL, Djamel ACHOURA a Nordine LEKLOU. Efficiency of high energy over conventional milling of granulated blast furnace slag powder to improve mechanical performance of

slag cement paste. *Powder Technology* [online]. 2017, **308,** 37-46. ISSN 00325910. Dostupné z: doi:10.1016/j.powtec.2016.12.014

[13] WALTERS, K., ed. *An Introduction to Rheology, Volume 3, 1st Edition* [online]. Elsevier Science. 1989. ISBN 9780080933696.

[14] GEORGE, Herman F. a Farrukh QURESHI. Newton's Law of Viscosity, Newtonian and Non-Newtonian Fluids. *Encyclopedia of Tribology* [online]. Boston, MA: Springer US, 2013, , 2416-2420. ISBN 978-0-387-92896-8. Dostupné z: doi:10.1007/978-0-387-92897-5_143

[15] MEZGER, Thomas G. *Applied Rheology: With Joe Flow on Rheology Road*. Anton Paar. 2018. ISBN 9783950401608.

[16] FEYS, Dimitri, Rolands CEPURITIS, Stefan JACOBSEN, Karel LESAGE, Egor SECRIERU a Ammar YAHIA. Measuring Rheological Properties of Cement Pastes: Most common Techniques, Procedures and Challenges. *RILEM Technical Letters* [online]. 2017, **2,** 129-135. ISSN 2518-0231. Dostupné z: doi:10.21809/rilemtechlett.2017.43

[17] DINKGREVE, Maureen, José PAREDES, Morton M. DENN a Daniel BONN. On different ways of measuring "the" yield stress. *Journal of Non-Newtonian Fluid Mechanics* [online]. 2016, **238,** 233-241. ISSN 03770257. Dostupné z: doi:10.1016/j.jnnfm.2016.11.001

[18] MøLLER, Peder C. F., Jan MEWIS a Daniel BONN. Yield stress and thixotropy: on the difficulty of measuring yield stresses in practice. *Soft Matter* [online]. 2006, **2**(4). ISSN 1744-683X. Dostupné z: doi:10.1039/b517840a

[19] ROUSSEL, N. *Understanding the Rheology of Concrete* [online]. 1st. Woodhead Publishing, 2011. ISBN 9780857095282.

[20] LU, Cuifang, *Zuhua ZHANG, Caijun SHI,* Ning LI, Dengwu JIAO a Qiang YUAN. Rheology of alkali-activated materials: A review. *Cement and Concrete Composites* [online]. 2021, **121**. ISSN 09589465. Dostupné z: doi:10.1016/j.cemconcomp.2021.104061

[21] YAHIA, A a *K.H KHAYAT. Analytical* models for estimating yield stress of high-performance pseudoplastic grout. Cement *and Concrete Research* [online]. 2001, **31**(5), 731-738. ISSN 00088846. Dostupné z: doi:10.1016/S0008-8846(01)00476-8

[22] JOLIN, Marc, *Dennis BURNS, Benoît BISSONNETTE,* Frédéric GAGNON a Louis-Samuel BOLDUC. UNDERSTANDING THE PUMPABILITY OF CONCRETE: Shotcrete for Underground Support XI. *Civil and Environmental Engineering Commons* [online]. Dostupné také z: https://dc.engconfintl.org/shotcrete/17

[23] ALONSO, M.M., *S. GISMERA,* M.T. BLANCO, M. LANZÓN a F. PUERTAS. Alkali-activated mortars: Workability and rheological behaviour. *Construction and Building Materials* [online]. 2017, **145,** 576-587. ISSN 09500618. Dostupné z: doi:10.1016/j.conbuildmat.2017.04.020

[24] A Basic Introduction *to Rheology: Whitepaper. Malvern* Instruments Limited [online]. , 1-20. Dostupné také z: www.malvern.com

[25] GIDDE, Ranjitsinha R *a Prashant M PAWAR*. On effect of viscoelastic characteristics of polymers on performance of micropump. *Advances in Mechanical Engineering* [online]. 2017, **9**(2). ISSN 1687-8140. Dostupné z: doi:10.1177/1687814017691211

[26] SALOMONSSON, Linda, *Gunnar STANG a Boris ZHMUD*. Oil/Thickener Interactions and Rheology of Lubricating Greases. STLE Tribology *Transactions* [online]. , 302-309.

[27] LEÓN-MARTÍNEZ, F.M., *P.F. de* J. CANO-BARRITA, L. LAGUNEZ-RIVERA a L. MEDINA-TORRES. Study of nopal mucilage and marine brown algae extract as viscosity-enhancing admixtures for cement based materials. *Construction and Building Materials* [online]. 2014, **53,** 190-202. ISSN 09500618. Dostupné z: doi:10.1016/j.conbuildmat.2013.11.068

[28] MAZZEO, Fred A. *Importance of Oscillatory Time* Sweeps in Rheology. TA Instruments [online]. 2019, 1(1), 1-4. Dostupné z: https://www.tainstruments.com/

[29] SCHULTZ,, M. *A. a L.* J. STRUBLE. USE OF OSCILLATORY SHEAR TO STUDY FLOW BEHAVIOR OF FRESH CEMENT PASTE. *Elsevier* [online]. 1993, **23**(2), 273-82. ISSN 0008-8846. Dostupné z: http://www.sciencedirect.com/science/journal/00088846

[30] KASHANI, Alireza, *John L. PROVIS, Greg* G. QIAO a Jannie S.J. VAN DEVENTER. The interrelationship between surface chemistry and rheology in alkali activated slag paste. *Construction and Building Materials* [online]. 2014, **65**(1), 583-591. ISSN 09500618. Dostupné z: doi:10.1016/j.conbuildmat.2014.04.127

[31] HAMADA, D., *T. HAMAI, M.* SHIMODA, M. SHONAKA a H. TAKAHASHI. Development of New Superplasticizer Providing Ultimate Workability. *International Concrete Abstracts Portal* [online]. Symposium Paper, 2006, **239**(1), 31-50. Dostupné z: https://www.concrete.org/publications/internationalconcreteabstractsportal/m/details/id/18369

[32] NÄGELE, E. *The zeta-potential of cement.* Cement and Concrete Research [online]. 1985, 15(3), 453-462. ISSN 00088846. Dostupné z: doi:10.1016/0008-8846(85)90118-8

[33] HABBABA, Ahmad a *Johann PLANK*. *Interaction Between* Polycarboxylate Superplasticizers and Amorphous Ground Granulated Blast Furnace Slag. Journal *of the American Ceramic Society* [online]. 2010, **93**(9), 2857-2863. ISSN 00027820. Dostupné z: doi:10.1111/j.1551-2916.2010.03755.x

[34] KELZENBERG, Anthony L., *Sharon L. TRACY*, Bruce J. CHRISTIANSEN, Jeffrey J. THOMAS, Matthew E. CLARAGE, Simon HODSON a Hamlin M. JENNINGS. Chemistry of the Aqueous Phase of Ordinary Portland Cement Pastes at Early Reaction Times. *Journal of the American Ceramic Society* [online]. 1998, **81**(9), 2349-2359. ISSN 00027820. Dostupné z: doi:10.1111/j.1151-2916.1998.tb02631.x

[35] PLANK, Johann, *Christof SCHROEFL, Mirko GRUBER,* Matthias LESTI a Roland SIEBER. Effectiveness of Polycarboxylate Superplasticizers in Ultra-High Strength Concrete: The Importance of PCE Compatibility with Silica Fume. *Journal of Advanced Concrete Technology* [online]. 2009, **7**(1), 5-12. ISSN 1346-8014. Dostupné z: doi:10.3151/jact.7.5

[36] LABBEZ, Christophe, *Bo JÖNSSON, Isabelle POCHARD,* André NONAT a Bernard CABANE. Surface charge density and electrokinetic potential of highly charged minerals: experiments and Monte Carlo simulations on calcium *silicate hydrate. J Phys* Chem B . [**online**]. 2006, 1(110), 9219-9230. Dostupné z: doi:10.1021/jp057096+

[37] STEINS, Prune, *Arnaud POULESQUEN, Olivier DIAT* a Fabien FRIZON. Structural Evolution during Geopolymerization from an Early Age to Consolidated Material. Langmuir [online]. 2012, 28(22), 8502-8510. ISSN 0743-7463. Dostupné z**:** doi:10.1021/la300868v

[38] SHI, Caijun a *Robert L. DAY.* A calorimetric study of early hydration of alkali-slag cements. Cement and Concrete Research [online]. 1995, 25(6), 1333-1346. *ISSN 00088846.* Dostupné z: doi:10**.**1016/0008-8846(95)00126-W

[39] BOSTRÖM, M., *V. DENIZ, G.*V. FRANKS a B.W. NINHAM. Extended DLVO theory: Electrostatic and non-electrostatic forces in oxide suspensions. Advances in Colloid and Interface *Science [online]. 2006,* 123-126, 5-15. ISSN 00018686. Dostupné z: doi:10.1016/j.cis.2006.05.001

[40] SCALES, Peter J., *Stephen B. JOHNSON*, Thomas W. HEALY a Prakash C. KAPUR. Shear yield stress of partially flocculated colloidal suspensions. AIChE Journal [online]. 1998, *44(3), 538-544*. **ISSN** 00011541. Dostupné z: doi:10.1002/aic.690440305

[41] FRANKS, George V. *Zeta Potentials and Yield* Stresses of Silica Suspensions in Concentrated Monovalent Electrolytes: Isoelectric Point Shift and Additional Attraction. Journal of Colloid and Interface Science [online]. *2002, 249(1),* 44-51. ISSN 00219797. Dostupné z: doi:10.1006/jcis.2002.8250

[42] SHI, Caijun, *A. Fernández JIMÉNEZ a* Angel PALOMO. New cements for the 21st century: The pursuit of an alternative to Portland cement. Cement and Concrete Research [online]. *2011, 41(7),* 750-763. ISSN 00088846. Dostupné z: doi:10.1016/j.cemconres.2011.03.016

[43] DAI, Xiaodi, *Serdar AYDıN, Mert Yücel* YARDıMCı, Karel LESAGE a Geert DE SCHUTTER. Effects of activator properties and GGBFS/FA ratio on the structural build-up and rheology of *AAC. Cement and Concrete* Research [online]. 2020, 138(106253), 1-14. ISSN 00088846. Dostupné z: doi:10.1016/j.cemconres.2020.106253

[44] ÖHRLUND, Åke. *Evaluation of Rheometry Amplitude Sweep* Cross-Over Point as an Index of Flexibility for HA Fillers. Journal of Cosmetics, Dermatological Sciences and Applications [online]. 2018, 08(*02), 47-54*. ISSN 2161-4105**.** Dostupné z: doi:10.4236/jcdsa.2018.82008

[45] GHOSH, Kushal a *Partha GHOSH. Effect of* Alkali Concentration on Mechanical Properties, Microstructure, Zeta Potential and Electrical Conductivity of Thermally Cured Fly Ash -Blast Furnace Slag Based Blended Geopolymer *Composites. Oriental Journal of* Chemistry [online]. **2018,** 34(2), 704-715. ISSN 0970020X. Dostupné z: doi:10.13005/ojc/340212

6 LIST OF TABLES

Table 1: typical chemical analysis results of GBFS obtained from national slag association (NSA, 2016) 14
Table 2: Phase composition of ground granulated blast furnace slag used in (%). 33
Table 3: Chemical composition of the granulated blast furnace slag used in (%). 33
Table 4: Composition of alkaline activators used in (%). 34
Table 5: Weights for 100 cm3 of GGBFS pastes using 144.05 g slag, slag volume fraction in paste 0.50 used (in g) 34

7 LIST OF ABBREVIATIONS AND SYMBOLS

1. AAMs – Alkali-activated materials
2. AAS – Alkali-activated slag
3. OPC – Ordinary Portland cement
4. CS – Calcium silicate
5. GGBFS – Ground granulated blast furnace slag
6. LVE – Linear visco-elastic region
7. CSD – Controlled shear deformation
8. CSS – Controlled shear stress
9. DLVO – Theory named after Boris Derjaguin, Lev Landau, Evert Verwey Theodoor Overbeek
10. G* – Complex modulus
11. G′ – Storage modulus
12. G″ – Loss modulus
13. tan(δ) – Loss factor
14. SWG – Sodium waterglass
15. PWG – Potassium waterglass
16. SH – Sodium hydroxide
17. PH – Potassium hydroxide
18. SC – Sodium carbonate
19. PC – Potassium carbonate

8 IMAGE LIST

Figure 1: A brief diagram of the blast furnace. 12
Figure 2: Graphical representation of the Bingham model [15]. 18
Figure 3: Modified Bingham plastic model rheogram [15]. 18
Figure 4: Herschel-Bulkley model for the yield point [15]. 19
Figure 5: *Stress and strain wave relationships for a purely elastic (ideal solid), purely viscous (ideal liquid) and a viscoelastic material* [24]. 20
Figure 6: Complex shear modulus (G), storage (G'), and loss (G'') moduli and phase difference (δ)* [25]. 20
Figure 7: A schematic representation showing how the LVE region is located in the amplitude sweep experiment. (Obtained from: https://www.netzsch-thermal-analysis.com) 21
Figure 8: Results of two amplitude sweeps, the functions of G' and G" show constant plateau values within the LVE region. Left: G' > G" in the LVE region, thus the sample has a gel-like or solid structure. Right: G" > G' in the LVE region, thus the sample is fluid [15]. 22
Figure 9: Typical plots of amplitude sweep test results. (A) Storage modulus G'and loss modulus G" against strain amplitude. (B) G' and G" against shear stress [27]. 22
Figure 10: Frequency sweep preset, where a controlled shear deformation is demonstrated by increasing or decreasing the frequency in several steps [15]. 24
Figure 11: Yield stress of the alkali-activated slag pastes with (a) $2.25 \cdot 10^{-4}$ and (b) $4.5 \cdot 10^{-4}$ moles M_2O/g slag, and slag paste without activator, as a function of time after initial mixing [30]. 25
Figure 12: Time-dependent zeta potentials of slag samples dispersed in DI water [33]. 26
Figure 13: Time-dependent pH values of slag samples dispersed in DI water [33]. 27
Figure 14: Time-dependent evolution of Ca^{2+}, K^+, and Na^+ concentrations in pore solutions from slag samples suspended in DI water (w/s ratios: 0.55 for slag # I, 0.52 for slag # II, and 0.46 for slag # III) [33]. 27
Figure 15: Schematic illustration of the electrochemical double layer that forms at the surfaces of slags # I (left) and # III (right) dispersed in water, and their surface charge as shown by the zeta potential [33]. 28
Figure 16: Zeta potential of slag suspensions in water (3 wt.%) after addition of different activator dosages [30]. 29
Figure 17: Relationship between the square of zeta potential of slag suspensions at 0, 2.2, 4.4, and 6.6 x 10^{-4} mole Na_2O/g slag (as marked on each point) and the yield stress of sodium silicate-activated slag paste at w/c = 0.45 [30]. 31
Figure 18: Measured pH of 3 wt.% slag suspension in water immediately after addition of different activator dosages [30]. 31
Figure 19: This schematic illustrates electrostatic inter-particle forces at a high concentration of sodium silicate in a slag paste [30]. 32
Figure 20: Schematic diagram of mini-slump test cone geometry. 35
Figure 21:Results of two amplitude sweeps of potassium hydroxide-activated paste with a potassium ion concentration of 1 mol/dm^3: A) strain controlled test; B) stress controlled test. 36

Figure 22: Spread diameter of a paste with slag and activator dose mixed by using the high shear mixer. 38
Figure 23: Evolution of oscillation strain parameter of GGBFS paste activated at different activator concentrations..... 39
Figure 24:Evolution of storage modulus of GGBFS paste activated at different activator concentrations..... 40
Figure 25: Evolution of stress calculated by TRIOS software of GGBFS paste activated at different activator concentrations..... 41
Figure 26: General evolution of tangent delta of GGBFS paste activated at different activator concentrations with inside closure look at 0.29 – 0.42 tangent delta value. 42
Figure 27: Evolution of crossover stress parameter of GGBFS paste activated at different activator concentrations..... 43
Figure 28: Evolution of strain calculated by TRIOS software of GGBFS paste activated with different activator concentrations..... 44
Figure 29: Evolution of storage modulus of GGBFS paste activated with different activator concentrations..... 44
Figure 30: Evolution of oscillation stress of GGBFS paste activated with different activator concentrations..... 45
Figure 31: General evolution of tangent delta of GGBFS paste activated at different activator concentrations with inside closure look at 0.25 – 0.45 tangent delta value. 45
Figure 32: Evolution of crossover stress parameter of GGBFS paste activated with different activator concentrations..... 46
Figure 33: Effect of variation of different alkaline activators on zeta potential of alkali-activated slag samples. 47